On Orbit Performance of the Rossi X-ray Timing Explorer Proportional Counter Array

K. Jahoda [1], J. H. Swank [1], B. Rossi [2], and ...

DRAFT 24 March 1998

ABSTRACT

The Rossi X-ray Timing Explorer was launched on 30 December 1995 with three X-ray instruments. We present on orbit performance and calibration results from the Proportional Counter Array (PCA).

1. RXTE mission

The Rossi X-ray Timing Explorer was launched on 30 December 1995 into a nearly circular orbit at 22 degree inclination. The apogee and perigee are 580 and 560 km; the precession of the perigee has a 30.2 day period; the orbit plane precesses with a 53 day period. (check with Frank) The orbit is predicted to last more than 8 years (Jean?). The mission is now in its third year of operation, and has entered the "extended mission" phase.

2. Description and Operation

The Proportional Counter Array (PCA), developed in the Laboratory for High Energy Astrophysics at the Goddard Space Flight Center, consists of 5 sealed Xenon-Methane proportional counter units (PCU) with unobstructed collecting area of $\sim 1400\,\mathrm{cm}^2$ each. Construction, ground performance, and early inflight performance are described by Glasser et al 1994, Zhang et al 1994, and Jahoda et al 1996. An integral part of the PCA, from the perspective of the user of RXTE data, is the Experiment Data System developed at the Center for Space Research at the Massachusetts Institute for Technology (reference?). Every event generated by a PCU passes 19 bits over a serial interface to the EDS. The information includes 8 bits of pulse height for events occuring on the xenon signal or propane veto layers, 2 bits of pulse height for events on the xenon veto layer, 8 lower level discriminator bits and a very large event flag. The EDS applies a time-tag and performs event selection and data compression to fit into the telemetry stream. The EDS is capable of performing up to six independent data compressions simultaneously. Of particular

[1]Laboratory for High Energy Astrophysics, Goddard Space Flight Center, Code 662, Greenbelt MD 20771

[2]MIT, Center for Space Research

interest, two standard compression modes have been run throughout the entire mission. Standard 1 provides light curves with 0.125 sec resolution and calibration spectra with full pulse height information collected every 128 seconds. Standard 2 provides pulse height information for each layer of each detector with 16 second resolution and 29 rates which account for all the "non-xray" events. Both Standard modes count each event produced by the PCA exactly once.

Both Standard modes run continuously except for resets which occur during SAA passages. This feature allows observers to examine the light curve as the satellite slews onto a source, which is occasionally useful in crowded fields (ref to Stark on J1744 light curve?). The start and stop times for all other modes are determined by "planning events", i.e. the predicted times for various spacecraft events, such as arriving on source or going into occult, which are then rounded to the nearest minute.

2.1. PCA configurations

Aside from data compression for telemetry, there are relatively few commandable items on the PCA; only two items are routinely selectable by observers.

The high voltage is, by design, commandable over a wide range. There are 16 commandable levels for both propane and xenon volumes. The xenon voltages are near 2000 V with 20 V steps while the propane voltages are near 2800 V with similar steps. The lowest commandable level is about 1000 V lower, chosen so that no multiplication occurs. The design allowed for the possibility that the gain would increase (for instance due to a slow leak) or decrease (due to poisoning of the gas). The default high voltage has been changed twice during the mission in order to reduce the frequency (PCU 3 and 4) or forstall the onset of occasional breakdowns (PCU 0, 1, and 2) (see below). The nominal high voltage settings over the course of the mission are given in Jahoda et al 1996. The PCA housekeeping data contains the instantaneous high voltage.

Each detector is equiped with a High Rate Monitor, which disables the high voltage when the total number of counts on any anode exceeds a preset counting rate for 3 consecutive 8 second intervals. The default is set to 8000 count/sec. This rate is occasionally adjusted upwards (typically to 24000 count/sec) for observations of extremely bright sources (there have been occasions when Sco X1 has tripped off the PCA detectors). It is unlikely that the HRM would ever be tripped if set much above 35,000 count/sec as paralyzable deadtime losses prevent the detector from registering more than about this counting rate.

Each detector is also equiped with a selectable Very Large Event window. Events which saturate the pre-amplifiers cause ringing as the amplifier relaxes towards the baseline; often the ringing can cause flase events to be pushed through the system. The timing of these events is dependent on the actual pulse height of the saturating event. Each detector has 4 commandable windows, set nominally to 20, 60, 150, and 500μs . The pre-launch intention was to allow "extra clean data" for very faint sources and "high throughput" data for very bright sources. The

size of the VLE window does affect the shape of the power spectrum (see below). During early observations of Cyg X1, with the VLE window set to 20μs , we observed a failure in layer 2 of detector 3 (? I think; check data from Barry's times). The nature of the failure is extra counts in a particular pulse height range in one of the channels. The rate appears variable and up to 4 count/sec; the detailed cause is not understood. The shortest window has not been used in the meantime. The default window, which appears adequate for most observations, is 150μs . Observations of some bright sources are conducted with the 50μs window.

2.2. EDS

2.2.1. Gain and Offset parameters

The gain of each of the PCU detectors is similar, but not identical. Because it is often desirable to co-add data from the 5 detectors, to maximize time resolution within a given telemetry budget, the EDS does some channel shifting in order to add more nearly equivalent energies. The EDS does integer arithmetic, parameterized by a gain and offset, to shift the 256 input pulse height channels to 256 corrected pulse height channels. The gain term always results in a compression, with the result that most channels are shifted upwards, but many pairs of adjacent original channels are shifted into corrected channels separated by two channels. (Check that we really are "stretching" everywhere.) This effect is modelled by the response matrix generator. The gain and offset parameters are not contained in the telemetry, but can be associated with the pulse height files with the ftool `pcagainset`. The channel shifting algorithm is

$$\mathrm{I}_{corr} = \frac{(\mathrm{I}_{orig} \times (256 + gain) + 128)}{256} + offset \qquad (1)$$

where I_{orig} is the pulse height produced by the PCU and I_{corr} is the corrected pulse height (Jahoda et al 1996). Table 1 has the values of gain and offset parameters used throughout the RXTE mission.

3. Long Term Stability

Long term gain and resolution stability can be continuously monitored for each detector by making use of tagged calibration events. Each PCU contains an Am^{241} source which decays by emitting an alpha particle and a characteristic X-ray. Any event which consists of an alpha particle flag and one additional lower level discriminator is binned into a calibration histogram, and telemetered once every 128 seconds as part of the continuously present Standard 1 data. Figure 1 shows the calibration events detected in PCU 0 during a 28,000 second interval in November 1996. The prominent peaks between channels 30 and 60 are Neptunium L lines, the peak near channel 70 is a 26 keV Americium decay line, the peak near channel 80 is a blend of an Americium line and a K-escape line associated with the 60 keV Americium feature visible near channel 155.

The rate of calibration events, summed over all six Xenon signal layers, is 3.33, 3.93, 2.66, 2.76, and 2.67 Hz for PCU 0, 1, 2, 3, and 4 respectively. Figure 2 shows the peak channel fit to calibration spectra for the fifth peak (near 30 keV) in each detector. Although there is a difference of about 10 channels from one detector to another, each detector shows stability over timescales of many months. We have selected about one observation per week for inclusion in this figure; each point represents (typically) $\sim$ 6 orbits. We selected data from blank sky pointings when available and from other observations of relatively faint (i.e. background dominated) sources to minimize all other potential sources of variations. (At very high rates, we expect the system gain to be depressed; see the section on energy response. At high rates, the calibration spectra will also suffer from deadtime losses, though this effect does not directly contribute to a gain shift). **This figure will have more data after suitable observations are chosen**.

Detailed examination of fig 2 shows that the gain has increased by $\sim 1\%$/year. We have fit a linear trend to the position of each of the Am^{241} peaks for each of the detectors and summarize the results in tables 3 (which gives the offset) and 4 (which gives the slope). The predicted channel on any given given day is simply offset + slope $*$ Day#. Day number is measured in Mission Elapsed Time, so day 1 corresponds to 1994 January 1 (XTE Time Tutorial). We do not distinguish by layer as we believe the small changes are due to a small loss of xenon in each detector which will affect the gain on all layers similarly.

Figure 3 shows the derived slopes for the 6 calibration lines as a function of effective energy (see Energy response section) along with a straight line fit. These data are from PCU 2, which has the largest gain changes, and are qualitatively similar to the data from each detector. The first order polynomial provides an excellent description, and has a significantly non-zero intercept. We use this parameterization to describe the gain change as a function of time.

3.1. Intermitent Breakdown

Beginning in March 1996, PCU 3 and 4 began to experience intermittent breakdown problems. While a detailed understanding of these events does not exist, we do know that once a detector begins to breakdown, it will remain in a breakdown state until it is turned off. We believe that periodic scheduled rest periods are beneficial, and we believe that the detectors should be turned off as soon as possible once a breakdown has been initiated. After a period of interim operations, PCA operations became predictable again after about June 1996.

We describe here several changes to the operating proceedure, all of which were in place by 1996 June (and some earlier). (or we could refer to SPIE 96 paper which documents all the operating changes).

The normal operating high voltage was reduced from 2030 V to 1990 V (Jahoda et al 1996). This results in an energy scale of about 3 channels (instead of 4) per keV (add second digit) and correspondingly less charge associated with each avalanche.

The high voltage is reduced to 0 instead of 1000 V during passages through the SAA. Although no multiplication takes place at 1000 V, charge is generated as energetic particles pass through the detector. If the anodes remain at 1000 V, the charge is collected there, and in fact showed up as a detectable (and occasionally very large) rate.

The orientation of the spacecraft has been slightly changed, so that the PCA is warmed slightly by the sun. The default roll angle is now 8 deg rather than 0 deg (check this).

PCU 3 and 4 are given pre scheduled rest periods when RXTE is observing targets that do not require the largest possible area. While no observer would choose 3 detectors rather than 5, many monitoring observations are systematics, and not statisitcs limited, and observations with 3 detectors have been adequate.

Most important, the EDS has been reprogrammed to continually compare the first moment of the pulse height distribution on anode L1 with that on R1, and similarly for the inner layers. There is no evidence that any breakdown has failed to set this trigger. Once set, the EDS sets a status indicator which is monitored in the space craft telemetry every 8 seconds. The spacecraft telemetry status monitor has been programmed to turn off the high voltage if the indicator is set for 5 sequential intervals. This in turn requires that the EDS set the indicator for 3 successive partitions (16 seconds for the Standard 2 data) which gets around almost all of the turn on and turn off transients (there is about one false alarm every other month, when a scheduled turn off, going into the SAA, triggers the TSM; this effect can occur on any detector). There have been no break down events on PCU 0, 1, or 2.

We believe that the scheduled rest periods lengthen the time between breakdowns, and it almost certainly helps ensure that the detectors are all on when large aperture is important and that two detectors are resting when not needed. There are of course trip-offs during periods when 5 detectors are desirable, and the standard analysis scripts recommended by the RXTE Guest Observer Facility now check for how many detectors are on.

Figure 4 shows the occurences of TSM tripoffs for PCU 3 and 4. The rate for PCU 3 has been relatively constant; PCU 4 has had two characteristic rates, and while originally was less prone to trip off than PCU 3, the opposite is now true. The breakdown rate has been approximately constant for both detectors for the last year. The detectors are typically disabled for $\sim 2.5 - 3$ hours after a breakdown. In percentage terms the loss of efficiency is relatively low, but the scheduled rest periods need to be factored in to get a complete picture.

4. Timing Calibration

Figure 5 gives a schematic representation of the timing logic within each PCU.

4.1. Deadtime

A detailed description of the effects of deadtime on a particular observation depends on both the source brightness and spectrum. The spectrum affects the ratio events observed in the first layer and other layers, and therefore changes the details of the intereaction of a paralyzable deadtime process (associated with each analog chain) and a non paralyzable process (the analog to digital conversion). Fortunately, a complete description is not always required. We present useful approximations for a common statistical representation of the data (power spectra) and for the construction of light curves.

4.1.1. Power Spectra

Even at relatively low count rates, the probability that events are missed has a significant effect on the shape of the power spectrum (Zhang et al 1995)

A period of deadtime can be generated by one of the following:

(1) An x-ray event: An x-ray event can cause the detector dead in two ways. First, it disables *its own* analog electronics, i.e., the CSA, SA, and the associated discriminators for a period of time which depends on the amount of energy it has deposited in the detector. Second, this event causes the ADC to be busy for $8.5\mu s$.

(2) A background event which can be either a charged particle or an x-ray: a background event cause the detector be dead exactly the same way as an x-ray if it occurs on one of the signal chains. If it occurs on one of the background chains, Vx or Alpha, it vetoes the detector for $6\mu s$. The detector is effectively dead during the $6\mu s$ because any event occurring, during this time, by definition, is rejected.

(3) A Very Large Event (VLE) which is an event that deposits more than 75keV of energy in any one or more of the 7 chains: L1-3, R1-3, and Vp. The VLE vetoes the entire detector for one of the four preselected times: 20, 55, 150, or $550\mu s$. During this veto time, no event is sent out to the EDS. The detector is effectively dead.

The Poisson random noise level is suppressed by the correlation between event caused by the deadtime. To a good approximation, the Poisson noise level with deadtime correction can be computed as follows:

$$P_{deadtime}(f) = 2[1 - 2r_0 t_d(1 - \frac{t_d}{2t_b})] - 2r_0 t_d(\frac{t_d}{t_b})cos(\frac{\pi f}{f_{Nyq}}), \quad (2)$$

where r_0 is the output event rate, t_b the bin size, t_d the deadtime, and f_{Nyq} is the Nyquist frequency.

To obtain acceptable fits, we need to include the contribution to the PSD by the VLE events. Since VLE events cause "anti-shots" in the data, its contribution can be written as

$$P_{vle}(f) = 2r_{vle}r_0\tau^2(\frac{\sin \pi\tau f}{\pi\tau f})^2, \tag{3}$$

where r_{vle} is the VLE rate, r_0 the good event rate, and τ the VLE window size which can take one of the four values: $20\mu s$, $55\mu s$, $150\mu s$, and $550\mu s$.

In practical fit to a power spectrum, one needs to add up equations 2 and 3.

add a figure?

4.1.2. Light Curves

Faint Sources

For the purposes of this discussion, a faint source is one where the deadtime correction is less than 10%. This includes the Crab. Dead time is produced by all events within the detector, and can be estimated from either Standard1 or Standard2 data. Both standard modes are designed to count each event presented to the EDS once. We illustrate this with data obtained while observing the Crab recently.

Figure 22 shows the total good rate (sum of the 5 rates from the individual detectors), the remaining counts rate, the propane rate, and the very large event rate. The data are collected into 8 second bins. The total rate is modulated by occulted periods, and is $\sim 13,000$ count/sec when on source. The remaining count rate is modulated at twice the orbital period (and is correlated with earth latitude, McIlwain L, or rigidity); in addition there is a contribution to the remaining count rate due to the source itself. This represents chance 2-fold coincidences of X-rays from the Crab. The rate of propane and very large events are also shown. All rates are summed over 5 detectors. (figures from /home/pcasrv2/keith/pca_cal_docs/deadtime; may need to be regenerated)

Figure 22 shows rates for the entire PCA; rates for each PCU are about one-fifth of the total. Each count contributes $\sim 10\mu$s to the total deadtime, except for the Very Large Event rate which typically contributes $\sim 150\mu$s. For the Crab, peak deadtime from all sources amounts to $\leq 6\%$.

Figure 23 gives the total rate (repeated from the earlier figure), the estimated total dead time, and the corrected total rate. The deadtime is estimated as the straight sum of the 4 terms above; no cross terms are included. The corrected rate is calculated as total/(1-deadtime). The 2 figures are identical except for the vertical axes. The simple prescription has removed most of the apparent variation in the rates observed from the Crab.

Deadtime corrections similar to this example will need to be performed for all observations attempting to measure relative flux variations to better than a few per cent. The time scales for background induced variation are about 45 minutes (half an orbit) although source variability can

cause variations in the deadtime on much faster time scales.

Bright Sources

We operationally define bright sources as those sources for which it is inappropriate to treat all incident events as independent. The definition is therefore dependent on how the data is used. For instance, for power spectrum analysis, deadtime must always be considered as the chance that events are miscounted or missed althogether changes the shape of the power spectrum. For the construction of light curves, on the other hand, the faint correction described above works well for sources with net counting rates $\leq 10,000$ Hz per PCU. (right number?) At higher count rates it is important to correct for the chance that two cosmic photons are simultaneously detected in different layers (Jahoda et al 1998) or that two photons are simultaneously detected in the same layer (Tomsick and Kaaret 1998).

bright sources (Rome) should pile-up have been accounted for too?

5. Absolute Timing

Accuracy of the RXTE absolute timing capability on scales longer than 1 second has been verified by comparison of burst arrival times with BATSE. We have used both bursts from J1744-28 and a bright gamma-ray burst (960924) which produced a large coincidence signal in the PCA to establish this agreement. All information on times finer than 1 second is contained within individual EDS partitionss. The relationship between EDS partitions and spacecraft time has been verified through ground testing and correlation of time tagged muon data with PCA data containing signals from the same muons. The content of the RXTE telemetry, and the relation to absolute time, has been thoroghly documented by Rots et al 1998 and references therein. The telemetry times in the RXTE mission data base give times that are accurate to $\leq 100\mu$s and users who require times $\leq 10\mu$s can achieve this by applying correction terms which are measured several times a day by RXTE mission operations personel. (where are the corrections stored in the data? faseBin?)

6. Energy Response

In this section we provide a description of all of the physical processes and approximations that are modelled in the response matrix generator `pcarmf v3.0` (ftools ref). Appendix A describes the detailed usage of this tool. PCA response matrices map 900 energies spaced from 0.023 to 100 keV (i.e. from well below to well above the range where the PCA has good efficiency) to 256 channels indexed from 0 to 255. Half of the energy channels are equally spaced below 10 keV, except that the three channels which include one of the Xenon L edges are split into two channels with the channel boundary matching the atomic edge. The remaining channels are

also equally divided except that the channel including the Xenon K edge is again split into two channels. A 256 channel "row" of the matrix gives the relative probability that a photon with of a particular incident energy will be observed in a particular channel. The sum of the 256 channels is typically less than unity and the sum over the row may be interpretted as the quantum efficiency at the energy in question.

An introduction to the principles of operation of proportional counters, with an emphasis on energy response, is given by Fraser 1989.

Figure 6 gives the flow for calculating the response to a particular energy. In the rest of this section we discuss all of the terms in the figure, emphasing which are accesible to measurement, which are available from the literature, and which are estimated or calculated in an ad-hoc manner.

6.1. Detector Efficiency

Each PCU detector, from the top, consists of a thermal shield, a collimator, an aluminized mylar window, a propane volume, a second aluminized mylar window, a xenon volume segmented into four separate volumes, and the detector body. A cross sectional view is presented in Glasser et al 1994 and an exploded view in Zhang et al 1994. Table 5 gives the nominal dimensions and characteristics of each layer. For generating the response matrix, however, the important quantity is the photo-electric stopping power of each layer and all exterior layers, which is estimated from the elemental composition and the areal density ($\mathrm{gm\,cm^{-2}}$).

The response generator accepts, as input parameters, the areal density of mylar and aluminum (assumed to be equally divided among the two windows), propane, and xenon in each of the three signal layers. (We neglect the thermal shield, which has a small stopping power compared to the mylar windows.) In principle, the areal density of each of the xenon layers could be calculated from the detector geometry. The second and third layers should be identical, and the first layer somewhat thicker (see fig 4 in Glasser et al 1994). The exact ratio must be calibrated, as we cannot measure the bowing of the inner window into the propane volume. This bowing may be different from PCU to PCU as the pressure history of each window is somewhat different. During the assembly of the first few detectors, the inner window was allowed to support 1 atmosphere. Although the mylar easily withstands this pressure differential over the 1.2×6.7 cm openings, it is permanently deformed. The filling procedure was eventually changed so that the inner window was never subjected to differential pressures greater than 100 torr. Rather than reproducing the detailed pressure history of each window, we have chosen to try to calibrate the areal densities.

Xenon is known to diffuse slowly into the propane volume, so it is also necessary to account for a time dependent xenon concentration in the propane layer. Figure 7 shows, for PCU 2, the ratio of observed counts in the front layer for data obtained during observations of the Crab in April 1996 and January 1998. We have simply divided the observed counts in each channel

(ignoring the small gain change). At higher energies, the observed counting rate is quite similar, while below $\sim$ 6 keV, we observed a higher counting rate in the earlier data set. We attribute the "missing" counts in the later data set to be photons absorbed in the propane layer by an increasing amount of xenon.

There are other possible reductions in efficiency, which have to do with the chance that a signal is produced in more than one signal layer. The initial photo-electron may travel into an adjacent cell before the kinetic energy has been completely thermalized. This depends on the electron range, which is energy dependent, and the detector geometry. We parameterize the unvetoed fraction as

$$f = 1.0 - p1 \times (E/E_o)^{p2} \tag{4}$$

with default values of $p1 = 0.015$, $E_o = 16$ keV, and $p2 = 1.86$. *For reasons I don't understand, p2 is hard coded, and will be made into a parameter in v3.1.*

Above the Xenon K edge, most interactions result in an escape photon, which escapes from the detector with high probability. Some of the escape photons are reabsorbed within the detector; if this happens on a different signal chain, the event will be vetoed (a reduction in efficiency) while if the reabsorption happens in the same signal chain, the photo peak will be slightly enhanced relative to the escape peaks. All of these probabilities are dependent on the details of the detector geometry; parameters which describe all these probabilities are described in the redistirbution section and the appendix.

Figure 8 shows the quantum efficiency for each of the 4 layers (propane and three xenon layers) for detector PCU 0. The two efficiencies for the propane and xenon first layer are shown for May 1, 1996 and January 1, 1998; the inner xenon layers are shown only for 1998.

6.2. Energy Scale

The Am^{241} calibration source provides easily measurable lines at characteristic energies between 13 and 60 keV (fig 1). Table 2 gives the energies. Unfortunately, most cosmic photons detected by the PCA occur at energies below 13 keV, so an extrapolation would be needed. We have several other sources of information. In the front layers, the Iron line from Casieopea-A (spelling?) is easily detected, and has been observed at all high voltage settings. Figure 9 shows the count spectrum observed in the vicinity of the Iron line for PCU 0 during high voltage epoch 3. The Xenon Lα escape line can also be observed if data is collected in a mode which accepts events which trigger exactly two signal chains. Some events create an Lα photon which is reabsorbed in a neighboring signal chain volume, and which is analyzed by the pulse height processing (see the block diagram in the timing section). During the regularly scheduled observations of blank sky (once per month since 1996 November and once per three weeks since fall 1997; the frequency was increased in order to get away from the 30 day period of the perigee precession) calibration spectra are collected in this mode. Unfortunately, the statistical precision of the determination of

the peak channel for the Xenon Lα is much less than for the calibration lines at higher energies.

For the second and third layers, we use the xenon transmission, as there is an enormous Xenon edge at 4.78 keV due to Xenon present in the outer layers. Figure 10 shows the count spectra from the Crab Nebula from layer 2 and 3 for PCU 0 (high voltage epoch 3). Although orders of magnitude down from the first layer, there is a measurable, and useful, transmission below the Xenon absorption edge at 4.78 keV, which allows a calibration in this region.

The most complicated part of the response matrix is the proper determination of the mean channel which corresponds to a particular input photon energy. As the name suggests, the pulse height produced in a proportional counter is approximately proportional to input energy, but the relationship between input energy and output mean channel is not linear, or even monotonic. Discontinuities occur at the atomic absorption edges, and can be understood in terms of a simple model. Each photo-electric interaction converts photon energy into electron kinetic energy and atomic potential energy. If energetically allowed, it is probable that the photo-electric interaction will remove an inner shell electron. Therefore, as the photon energy crosses an atomic edge, there will be a large increase in the amount of energy initially converted to atomic potential energy. The atom quickly relaxes to its ground state through a variety of processes (see Dias et al 1997 for a detailed discussion of the processes in Xenon); of interest here is that the resulting ion is, on average, more highly ionized than for the interactions just below the edge. A result of this is that less electrons are produced to participate in the proportional counter avalanche as some of the photon energy is lost to creating the Xenon ion.

The relationship between input number of electrons and mean channel, on the other hand, is approximately linear, and certainly has no large discontinuities. We take advantage of the detailed studies and monte carlo results available for Xenon (Dias et al 1997, Santos et al 1994a, Santos et al 1994b) which parameterize the average energy required to create one electron as a function of photon incident energy. The values of $w(E)$ are all near 22 eV, but with sudden discontinuities at the Xenon absorption edges and gentle variations inbetween. Although the Monte Carlo results appear to work well on both sides of the Xenon L-edge, Dias et al 1997 compares the predicted jump to that measured by several groups and concludes that the model overpredicts the measurements by about a factor of 2 at the L3 edge. We adopt an *ad hoc* definition of $w'(E) = 22.0 + (w(E) - 22) * 0.5$. This maintains the variation with energy, but reduces the apparent jump at the L edge significantly. Similarly, we define an effective energy $E' = 22 * E/w'(E)$, which has the features that $E' \sim E$ and (to the extent that w'(E) is a good description of the average energy required to produce an electron) E' is strictly proportional to the number of electrons produced in the gas. Figure 11 shows the values of $w'(E)$ we adopted. Note that all of the values are close to 22 eV per electron, but with noticeable jumps at the edges and slow variations in between.

We could easily add a knob that allows the tuning of the 50% parameter; that will be version 3.1 unless 3.0 bounces for some code reason. Adjusting the parameter should not be done with also

thinking about the energy-to-channel relationship

We have determined the energy to channel relationship for each detector, in a period corresponding to the begining of the third high voltage epoch (Jahoda et al 1996) in several steps. We took the peak positions of the Am^{241} lines along with the peak for the Xenon Lα line. We fit the peak channel as a quadratic function of E', and artificially reduced the error associated with the Xenon Lα line to force our fit through this point. This was done separately for each layer. We examined the apparent energy of the Cas A Iron line in the first layer, and perturbed the assumed peak channel for the Xenon Lα line and repeated the process until the Iron line was observed at 6.59 keV (Hatsukade and Tsunemi 1991, Holt et al 1994). On the inner layers we used the apparent peak in the pulse height spectra of fig 10 to select the best energy to channel relationship. We repeated the process for different values of the ad hoc constant which appears in our definition of $w'(E)$. We selected the definition of $w'(E)$ by choosing the value which gave the best fit to the Crab Nebula in the first layer; our determination was made *before* we bcame aware of the Dias et al 1997 result that $w(E)$ predicts too large a jump. The Dias et al 1997 results lend additional weight to our originally ad-hoc proceedure to reduce the jump.

The channel to energy relationship was independently determined for the initial parts of the mission with different high voltage settings. (reproduce the table from SPIE paper?). We account for slow gain changes using the relationships defined in table 3 and 4.

6.3. Redistribution Matrix

With the energy to channel relationship, we determine the channel which corresponds to the photopeak (C_o in fig 6). We determine the position of the escape peaks by subtracting, in channel space, the energy of the escape photon and adding an offset which accounts for the different mean potential energy left with the Xenon ion. We take the offsets from Dias et al 1996 *We observed the same phenomenon during ground calibration at the Brookhaven National Laboratory X-ray Synchrotron. (make figure?)*

The relative height of the escape peaks depends on both atomic physics and the detector geometry. The L escape fraction is small, at least partly because the L escape photon has a short mean free path in Xenon. The K escape fractions are large as these escape photons are both more likely to be produced, and more likely to get out of the detector. Figure 12 shows two channel spectra, obtained above and below the Xenon K edge during ground calibration runs at the Brookhaven National Laboratory.[3] The upper spectrum shows the pulse height obtained from 10.6 keV incident X-rays, with a barely discernable Lα escape peak. The lower spectrum has incident energy of 37.4 keV, and most of the detected photons are in the escape peaks.

[3]The high voltage setting is similar to epoch 1 of the RXTE mission; i.e. through 1996 March

Figure 6 gives a schematic weighting for the photopeak and the escape peaks. For energies above the K edge, we ignore the L escape peak. The peaks are modelled as gaussian, with a $\sigma = (1.06 + 0.051 \times E' + 2.4 \times 10^{-4} \times E'^2) \times S$ channels. The factor S is an input to the matrix generator; as there is no information about where in the detector an X-ray interacted, beyond the signal chain, the constant must account for the average resolution. For all data obtained in the third high voltage epoch (i.e. after 1996 April 14), S is 0.8 (Weaver et al 1998. Fig 13 shows the modelled response of layer 1 of PCU 0 to two lines: one at 6.5 keV, and a second line (100 times brighter incident flux) at 55 keV. The L escape line, while present, is barely visible in our model.

Partial charge collection is also a well known effect in proportional counters, particularly at low energies (Inoue et al 1978, Jahoda and McCammon 1988) where it can be successfully modelled as a competition between diffusion of the electron cloud in all directions and acceleration of the electrons towards the avalanche region. For the PCU, the approximation that all photo-ionizations occur near the window is less valid. We have implemented a crude partial charge collection algorithm in `pcarmf v3.0` which redistributes a portion of the events to lower pulseheights. The redistribution is uniform over all energies below the incident energy. The fraction that is redistributed is proportional to the ratio of $\sigma(E)/\sigma(5keV)$. The default value of the correction in v3.0 is 0.001 (i.e. small enough that this effect has effectively not been included). This will affect the accuracy of the matrices most noticeably at low pulse heights, particularly at energies where the observed number of counts/channel is less than about 10%?? of the peak count/channel. For the Crab, this is at energies $\leq$ 2.5?? keV. For the current matrices, our normalization for this effect is so small as to be not included.

6.4. Fits to Crab

7. Background

7.1. Characteristics

The overall background after rejecting all coincident events, from all sources, varies between 100 and 250. The background, limited to the first layer and in channels below 27 (i.e. energies below 10 keV) varies between 10 and 20 Hz while looking at the earth; an additional signal of $\sim 10Hz$ is observed from the sky. (figures being prepared in /xtepca/p13/bkgd/960703)

The RXTE satellite has been obtaining about a day of blank sky observations once a month since 1996 November, and about once every 3 weeks since 1997 September. The change in frequency was necessary to break an unintended synchrony with the 30 day period of the precession of the perigee.

Figure 18 shows the total observed rate from a day of blank sky observations obtained on 1997 March 31. We have chosen to show data from 3 detectors (PCU 0, 1, and 2) scaled to the rate that is expected from 5 detectors; these detectors were on for the entire day, while PCU 3

and 4 were deliberately turned off for part of this observation as described above. The binning is for 128 seconds; the errors are representative of the 3 detectors, and there is clear evidence of variations in excess of that allowed by counting statistics. The largest variations are correlated with passage through the South Atlantic Anomaly (SAA) and with latitude. Beginning half way through this day, the spacecraft is passing through the SAA and large short term enhancements are seen. There is also a term with a several hour half life, visible in the fact that the pedestal seems elevated for later passes through the SAA. During the non-SAA orbits, the overall variation is less, but strongly correlated with latitude, showing two peaks per orbit. The small spike in the light curve just past 70,000 seconds is due to a source that entered the field of view during a slew. (figure prepared in /xtepca/p13/bkgd/970331)

The presence of background components *after* passage through the SAA indicates that some part of the detector or spacecraft becomes activated. The RXTE spacecraft has one instrument which is on continuously, and which can therefore be of potential use in tracking total radiation dosage. This instrument is the HEXTE particle monitor (Rothschild et al 1998). Figure 19 gives the HEXTE particle monitor rate as a function of time through the first 20 (check time, expand?) months of the mission. The rate, reported once per day but averaged over 3 days at a time, shows three notable trends. There is a gradual increase with time; there is an apparently periodic modulation with 30 day period; and there is additional aperiodic variability. We have fit these data with a trend plus sinusoid; the best fit sine has a period of 30.1 days, which is exactly the precession of the perigee of the orbit. Since the amount of time per orbit that the satellite spends in the SAA is related primarily to the ascending node, and since the SAA has quite a large variaition with altitude, it is not surprising to find that the integrated dose varies based on whether the perigee is in the SAA regions. (figure 19 is based on /xtepca/p14/hexte_pm/fig3.qdp)

It is immediately clear however, that there are aperiodic variations in the SAA dose that are comparable to the periodic variations, and that over a year, the overall level can change by an amount similar to the periodic variation. It is difficult to infer the magnitude of the expected variations in the PCA event rate from this measurement of SAA protons, so we address the normalization experimentally below, expecting however, to find evidence for long term, periodic, and random changes in the background.

cube generating programs, etc., are in /xtepca/p14/hexte_pm

7.2. Background models

Background is subtracted from source data based upon a model of the background detected by the instrument rather than by direct measurement. In general, the modeled background spectrum can be based upon parameters measured at the time of the observation, parameters describing the condition and position of the spacecraft, and parameters describing the evolution of the spacecraft. In practice, the most significant contributions to the background are dependent upon the local

particle environment of the satellite and the recent history of passage through the SAA.

The local particle environment determines several counting rates which are routinely recorded along with PCA data so background which is caused by these particles is modeled based upon these parameters. Early models were based upon a measured rate called "Q6" (see the appendix on Standard 2 data) which is the rate at which 6 of a PCU's 8 discriminators (6 in the detector volume, 1 in the propane anti-coincidence layer and one in the xenon anti-coincidence layer) are triggered in coincidence. This rate is particularly sensitive to the local particle environment. It turns out, however, that the rate of "VLE's" (Very large events—events which trigger a discriminator set with a very high threshold.) is more strongly correlated with the measured background rate in the good PCA data so local background models are based on this rate alone. The VLE rate is, however, dependent on the source counting rate and is sensitive to sources which produce high-energy X-rays, so models based upon the VLE rate are most appropriate for faint or soft sources. Q6-based models must be used when analyzing bright, hard sources where the error introduced by using them is insignificantly small.

For the purposes of modeling the effect of activation of the spacecraft on the background rate, the spacecraft's orbit is decomposed into a coordinate system in which each point represents a unique history of SAA exposure. The two coordinates correspond to the longitude of the ascending node of the satellite's orbit (Called BKGD_THETA by the modeling tool, pcabackest) and the time since crossing the Equator at the ascending node point (Called BKGD_PHI). Under the assumption that fluctuations in the size and intensity of the SAA are not relevant to the SAA-induced background outside the SAA, these coordinates for a basis for a model of an activation-induced background component.

PCA background models based upon these parameters have been constructed in two ways: Using data from the blank-sky observations and using data from periods of Earth occultation. In both cases, the local particle parameter is divided into several rate bins for each detector anode chain and an average background spectrum is calculated from the available data for each bin. The models based upon the local particle parameter are constructed using data from only those spacecraft orbits in which the SAA-induced activation is small. (In practice, these are the orbits where $-60° < \mathrm{BKGD\_THETA} < 120°$.) Some of these data are still significantly contaminated by SAA-induced activation but this contamination can be later removed by an appropriately constructed model of the activation component of the background.

The activation component of the background model is constructed by dividing the two spacecraft orbit parameters (BKGD_THETA and BKGD_PHI) into bins and determining the average spectrum from the available background data for each bin and each detector anode. Early activation models were constructed only from data not using in constructing the local particle background models. The latest versions of these models, however, are constructed from all data to allow a correction for activation in the region of the spacecraft orbit space originally taken to be free from activation.

If a model is constructed from Earth occulted data, then a third model component must be used which represents the difference between the average blank sky spectrum and the average Earth-occulted spectrum. This component contains information about the diffuse X-ray background as well as a correction for the high-energy albedo of the Earth's atmosphere. Models constructed using Earth occulted data produce the same results as models constructed using blank sky data. The choice of which data to use in constructing the models are based on factors other than the relative quality of the constructed models.

A software tool, pcabackest, is provided to apply the background models constructed as described above to scientific data collected with the PCA. Pcabackest takes the as input data collected in standard mode 2, a *filter* file which contains collected parameters from many sources, and the background model files. It produces as output a file which is structured very similarly to the standard mode 2 file which was the input. The measured spectra of the standard mode 2 data file are replaced by spectra derived from the model files which represent the average expected background contribution to the input file. This background estimate file can be processed in a manner identical to that used to process the actual data to produce either a background spectrum or light-curve for subtraction from the collected data.

Figure 20 shows a nearly uninterrupted observation of IRAS 18325-5926 which lasted over 2 days in 1998 February. There are gaps for the SAA, and a few interuptions for brief monitoring campaigns; this source was in the continuous viewing zone during this period. The top panel shows the raw rate from the first layer of PCU 0, 1, and 2 in channels 51-249, a range where no signal is expected. The middle panel shows the predicted background from a VLE based model constructed from sky looking data obtained in 1997. The third panel shows the ratio. During the periods between SAA passes, the ratio remains near 1, indicating that the VLE dependence does a relatively good job predicting background. During the SAA periods, the ratio of data/model is much higher, giving a sense of the relative importance of the activation component.

7.3. Activation Corrections

Our current models cannot produce any aperiodic variability in the background, but all is not lost.

7.4. Data Selection

7.4.1. Electron contamination

The background models are parameterized in terms of particle rate. The Q6 rate and VLE rate (which are highly correlated) are related to energetic particles (primarily protons and alpha particles) which pass through the detector and leave ionization in many cells. Low energy

electrons, on the other hand, may lose all their energy within the detector. Electrons with several 10s of keV may come through the collimator and stop in the first xenon layer. The rate of propane plus first layer coincidences measures such a population, and while these events are vetoed, the rate can be used to screen periods when there may be increased background, for instance due to the same electrons flourescing the collimator. We define an "electron ratio" as (VpX1LCntPcuN + VpX1RCntPcuN) / (Q6VxVpXeCntPcuN) (see tablestd2) for discussion of the telemetry mnemonics). This ratio is quite similar from one detector to the next. Figure 21 shows the the electron rate (top panel), proton rate (middle), and their ratio. Although the particle rates are quite variable, they often track each other extrodinarily well, resulting in a flat ratio. Occasionally, however, there are large excesses in the electron rate, which can easily be screend out of the data. The measured rates are not, strictly speaking, direct measures of either electron or proton rate, so a physical interpretation of the value of this ratio (typically ≤ 0.1 during low electron periods) is not possible.

7.4.2. Time since SAA

8. Field of View

8.1. Collimator model

Each PCU has a collimated, approximately circular, field of view of radius 1° from peak to zero throughput. Each PCU has a collimator assembly made up of 5 individual collimator modules. Each module contains a large number of identical hexagonal tubes which provide the collimation and each module was aligned independently. Measurements of these alignments indicate that all modules of each PCU are aligned to within ?? arcmin. The opening of each individual hexagons is 0.125 inch (flat to flat) and 8 inch in length.

To model the on-orbit collimator efficiency we began with the theoretical transmission function for a perfectly absorbing hexagonal tube with dimensions equal to those comprising the PCA collimator modules. The fabrication, mounting and alignment of the collimator modules must introduce some level of misalignment among all the individual hexagons making up the collimator assembly for a given PCU. To produce a more realistic model than the perfect theoretical response for a hexagonal tube we averaged the responses from a large number of perfect hexagons but with the pointing direction of each tube randomly displaced from the vertical. The random offsets were parameterized with a single parameter, σ, which represents the width, in arcmin, of a gaussian distribution centered on the vertical from which the random offsets were sampled. Thus, the larger σ the greater is the spread in pointing directions of the individual hexagonal tubes. The geometry for calculation of the collimator model is shown in figure 14. The pointing direction is along the X_{RXTE} spacecraft axis. We calculate the model response by randomly drawing an off axis angle, θ, from a gaussian distribution centered on $\theta = 0$ and with a standard deviation σ. A random

value for the azimuthal angle ϕ is also selected. The theoretical transmission for this orientation is calculated and added to the total. The process is repeated for a large number of offsets, and the final total response is normalized to 1.0 at its peak. We calculated a series of models for different values of σ, ranging from 1 arcmin to 8 arcmin.

We used the Crab as an approximately constant and point-like source of X-rays in order to determine the best pointing direction for each PCU, the so called boresights, as well as the value of σ which gave the best fit to the scan data. The RXTE spacecraft attitude control system (ACS) computes an estimate of the spacecraft attitude on a 0.25 second timescale. The attitude information prescribes the orientation of the three spacecraft axes in Earth-centered inertial coordinates (epoch J2000). With this knowledge the location of any X-ray source with respect to the spacecraft coordinates can be calculated. We used the attitudes to determine the counting rate in each PCU from the Crab as a function of position in the spacecraft frame. We then minimized the function

$$\chi^2_j = \sum_i \frac{\left(O^j(Y^i_{RXTE}, Z^i_{RXTE}) - R^j M(Y^i_{RXTE} - Y^j_{bore}, Z^i_{RXTE} - Z^j_{bore}, \sigma)\right)^2}{O^j(Y^i_{RXTE}, Z^i_{RXTE})} ,$$

where O is the observed countrate, M is the model response, i denotes the individual rate and attitude samples, j denotes the different PCUs, Y^j_{bore} and Z^j_{bore} specify the pointing direction (boresight) of each detector, σ specifies the smearing of the ideal hexagonal response discussed above, and R^j denotes the peak countrate for each detector, that is the counting rate at the peak of the response. Since sources are effectively at infinity only the direction is relevant. The direction to the source with respect to the spacecraft frame can be uniquely specified with only two parameters. We elected to use the Y_{RXTE} and Z_{RXTE} coordinates as the independent variables. Since these form part of a unit vector we have that $X^2_{RXTE} + Y^2_{RXTE} + Z^2_{RXTE} = 1$. Before performing the fit we first corrected the observed rates for detector deadtime using the faint deadtime correction formula described above. For the Crab at full throughput we typically have a deadtime fraction of between 3 and 5 %. This deadtmine effect is larger than that due to unrejected detector background, which at about 20 cts/sec is less than 1%. We found that $\sigma = 5 - 6$ arcmin gave the smallest values of χ^2. Table 6 summarizes the derived values of Y^j_{bore}, Z^j_{bore}, σ_j and R^j for each detector based on our fitting. R^j is given as a relative rate, scaled to the detector with the highest throughput. **Tod, I don't have the σ values**

To asses the quality of the fits we performed an additional background fitting during some of the scans for which the backgrounds appeared flat across the entire scan profile. We then fit these individual, deadtime corrected and background subtracted scan profiles to the collimator models derived from the entirety of scans. We allowed the peak countrate to vary as the only parameter of the fits. Figures 15 shows one of the scan paths used in this analysis along with the model collimator response for detector 1. Figure 16 shows the countrate as a function of off axis position during this scan along with the best fitting model of the collimator efficiency. Figure 17 shows the residuals of the fit. The model is generally good within a few percent over most of the scan. These results are generally characteristic of those for each of the 5 PCU detectors.

8.2. Solid Angle

The linear approximation for the response, $f = 1 - r/r_0$ where r_0 is equal to 1 deg, overestimates the solid angle. Integrating $f(r)sin(r)d\Omega$ over $0 \leq \theta \leq 2\pi$ and $0 \leq r \leq r_0$, and keeping terms to order r_0^4 gives $(\pi/3.0)r_0^2(1 - r_0^2) = 0.000318897$ (for $r_0 = 1$ deg). This compares with 0.000320578 from integrating this response numerically.

Integrating the summed responses numerically for all the PCUs, using the model file pcacoll_v100.2, we get 0.00029703, or about 8% less.

This is approximately the effective solid angle of a linearly falling response out to r_0 if $r_0 = 0.965$ deg. Put another way, this is the solid angle you get by integrating a flat (unit) response from r= 0 to 0.55712 degrees.

We thank the tireless efforts of uncountable people. The Brookhaven National Laboratory National Synchrotron Light Source is supported by the U.S. Department of Energy under Contract Number DE-AC02-76CH00016.

A. Contents of the Standard Data types

Standard 1 telemeters a few rates with a 0.125 second resolution and Americium Calibration spectra for each signal layer with full pulse height and 128 second resolution. Table 7 gives a list of the column names associated with Standard 1 mode data in the RXTE data base. The first 5 rates are the total number of good events (single lower level discriminator) in each detector; The 1024 entries per row cover 128 seconds with a time resolution of 0.125 seconds. The next 3 rates (with identical time resolution) give the rate, summed over all 5 PCU, of all coincident events, all events which trigger only the propane layer, and all events which saturate the amplifiers and produce a VLE flag. Coincident events are carefully defined to include all events not counted elsewhere exactly once.

The columns labelled CalX3LSpecPcu0 contain the calibration spectra. LL runs over the six signal layers and take on values of 1L, 1R, 2L, 2R, 3L, and 3R while N runs over the PCU and takes on values from 0 to 4.

Spillage and Mode Specific provide EDS disgnostics. Under normal operations, these always assume values of **Ed M, help me here)**

Standard 2 telemeters pulse height spectra, individually by anode, with 16 second resolution as well as 29 coincidence rates per detector. Representative values of the column names in the RXTE data base are given is table 8. (Only column names for PCU 0 are shown; similar items exist for each detector). The first six items are 129 channel spectra from each xenon signal anode. The original 256 channels have

been compressed by combining channels 0-4 into 1 channel, telemetering channels 5-53 individually, channels 54-135 are added in pairs, channels 136-237 are added in triplets, 238-249 are added four at a time, and channels 250-255 are telemetered as a single channel. The 256 channel data from the propane layer are similarly compressed to 33 channels; the details of the compression are stored in the FITS headers, and can be decoded with the ftool `rddescr`.

After the spectral information, there are 29 coincidence rates telemeterd for each detector. The index column of table 8 merely provides a running index; we find this a convenience. When these 29 column names are specified as the input to the ftool `saextrct ... accumulate=many ...` the resulting columns in the light curve are named `RATEN` where `N` corresponds to index.

PCA housekeeping data is documented in Giles 1995. Some of the most useful spacecraft housekeeping data, including some instrument parameters, is gathered in the filter files (reference?).

A. Using PCA response matrix generator PCARMF v3.0

Creating a PCA response matrix involves creating a matrix suitable for each detector (using the ftool `pcarmf`), shifting the channels following the EDS gain and offset description(`rddescr`, `pcagainset`, and `gcorrmf`), rebinning the channels to match the telemetered pulse height bins (`rbnrmf`), estimating the effective area of each detector after accounting for point (`xpcaarf`), combining the area and redistribution matrices (`marfrmf`), and adding the matrices from the 5 PCU (`addrmf`). The perl script `pcarsp` takes care of these tasks. We describe here all the inputs to the fundamental matrix generator `pcarmf`.

Table 9 gives the parameters which are input to pcarmf. Column 1 gives the mnemonic, column 2 the behaviour of the tool (i.e. whether the parameter is queried for or a default taken if not specified on the command line), and the default value.

Several parameters are always prompted for. These include the name of the output file (`outfile`), the PCU identification (`pcuid`) which can take on values from 0 through 4, the date of the observation (`date`) which is entered as an integer in yymmdd format, and the signal chain in question (`lld_code`). The signal chain is coded as a number between 1 and 64 where we have assigned a value of 1,2,4,8,16,32, and 64 to the signal chains L1, R1, L2, R2, L3, R3, and VP (Glasser et al 1994 illustrates these designations). In addition to all of these values, sums are allowed: 3 indicates the sum of both front layers L1 and R1 while 63 indicates the sum of all xenon layers. The energy to channel relationship can be parameterized as a quadratic in energy (`e2c_model = 2`) or in effective energy (e2c_model = 3). Model 2 is not

supported in the sense that the calibration data base contains no coefficients for this parameterization.

The energy to channel coefficients are typically obtained from the calibration data base (the default value of `e2cfile=CALDB`) although the user can supply a calibration format fits file with similar information or the user may specify `nofits=1 e2cfile=myfile` where `myfile` is a fixed format file with entries in this format:

```
960414  0  03  3 -5.8585E-01  2.7908E+00 -2.5328E-03
```

The 7 entries are `date`, `pcuid`, `lld_code`, `e2c_model`, and three coefficients of the quadratic relationship between effective energy and channel number. These values are read with a formatted FORTRAN read statement expecting formats (a1,1x,i6,i3,i4,i3,10(1x,1pe11.4)) (If the first character of any line is "c", the line is ignored). The file is read until a date less than the requested date is found with appropriate values for `pcuid`, `lld_code`, and `e2c_model`. In the special case where `lld_code=63`, `pcarmf` obtains coefficients for the three layers `lld_code=3,12,48` separately, evaluates all three matrices and adds the results.

The user can supply an energy dependent correction to the effective area by specifying `scale_hack=1 scale_file=eff.area.ratio`. The file `eff.area.ratio` should contain up to 129 energy/value pairs; the value is the fractional correction to the effective area. Straight line interpolations are performed at all intermediate energies, and no correction is made at energies below the first or above the last value. The default behaviour is to apply no correction.

The `chatter` and `clobber` parameters have the usual ftool definitions and control the verbosity of the screen output (`pcarmf` is relatively taciturn under all circumstances) and whether the output file will overwrite an existing file.

All of the parameters described above change the operation of the response generator; the rest of the parameters have to do with characteristics either of Xenon physics or the PCU detector geometry.

The photoelectric efficiency of the detector is determined by the thicknesses of mylar, aluminum, propane, xenon and methane in the detector. For detector N (N=0 to 4) the amount of material in the front volume (i.e. the effective window) is specified by `my_gmcm2_pN`, `al_gmcm2`, and `pr_gmcm2` which give the amount of mylar, aluminum, and propane in $\mathrm{gm\,cm^{-2}}$ along with three parameters which together specify the amount of xenon in the propane layer. The three parameters are the initial amount (`xe_gm_cm2_prN`) in $\mathrm{gm\,cm^{-2}}$, a reference date (`date0_N`), and a daily change (`xe_pr_daily_changeN`) in $\mathrm{gm\,cm^{-2}\,day^{-1}}$. Default values used with version 3.0 of `pcarmf` are given in table 9.

The amount of material in the three main signal layers is specified by xe_gm_cm2_lM_pN where M runs from 1 to 3 with 1 being the front layer. No provision is made for a decreasing amount of Xenon as this has a very small effect on the pressure. The propane volume has 0.1 the gas volume of the Xenon layer, so even though the extra xenon in the propane layer must be due to diffusion from the xenon layer, the partial pressure change is a factor of ten lower in the main volume (this is likely the cause of the gain increase documented in tables 3 and 4; the small pressure change affects the gain much more strongly than the photoelectric efficiency.)

The energy of the three Xenon L-edges and the Xenon K-edge are specified by xeKedge, xeL3edge, xeL2edge, and, xeL1edge. These are used to adjust the channel boundaries on the matrix input to avoid having matrix energy channels of both sides of an edge.

The escape fractions (the weights in fig 6) are specified by EscFracKb, EscFracKa, EscFracL1, EscFracL2, and EscFracL3. Here the distinctions are between Kα and Kβ escape peaks and between Lα escape peaks which originate from events in the first, second, or third layer. Because of the short mean free path of the Lα photon, the escape fraction defaults to 0.0 on the second and third layers. (Version 3.0 also reads EscFracLt, originally the escape fraction for lld_code=63 but now unnecessary since this case is taken care of by adding the redistribution matrices for the three layers together.) The parameter xe_kedge_veto gives an an hoc correction to the total photo electric efficiency above the Xenon K edge. The net efficiency is equal to the photoelectric efficiency times xe_kedge_veto (i.e. the self vetoed fraction is $(1.0 -$ xe_kedge_veto$)$).

The position of the escape peaks is determined by the escape photon energies EscEnerKa, EscEnerKb, and EscEnerLa (in keV) and the offsets that account for energy actually released into gas ionization delta_el_Ka, delta_el_Kb, and delta_el_L (in electrons). The offset can be converted to eV by multiplying the offset by $w'(E)$ shown in fig 11. (The parameters DeltaE_L1, DeltaE_L2, DeltaE_L3, and DeltaE_K are not currently used; these, or something similar, are necessary if the channel to energy relationship is parameterized as a simple polynomial function of energy. We have chosen instead to parameterize the discontinuities in the channel to energy relationship through the discontinuities in the E to E' relationship.)

The inputs epoint and track_coeff specify E_o and $p1$ in eq 4. Pcarmf v3.0 hard codes the value of $p2$ to 1.86; this will be a parameter in version 3.1 and later

The resolution is calculated internally in channels. High voltage epoch 3 (i.e. most of the mission) requires resolution_factor=0.80 (the default); high voltage epoch 1 requires resolution_factor=1.00. *use some Cas A data to check on this.* The partial charge correction is normalized by pcc_coeff=0.001, which gives the magnitude at

5 keV. The entire response is reduced by the fraction pcc_coeff and these counts are redistributed equally at all energies below the photopeak. At other energies, the normalization is pcc_coeff$(\sigma(E)/\sigma(5)$ where $\sigma(E)$ is the xenon photoelectric cross section at photon energy E. If the calculated normalization is greater than 0.10, it is arbitrarily set to 0.10.

The gain change is parameterized, for each PCU (from 0 to 4), by gain_shift_offsetN, gain_shift_slopeN, and date0_N (note that the reference day is also used in the calculation of xenon in the propane layer). The gain shift and offset values are per day; the first two coefficients in the energy to channel relationship are slightly modified. Our experience with the Crab is that using a matrix suitable for 1996 April for analyzing data from 1998 January creates the appearance of a line feature near 5 keV due to the mismatch between the actual channel and modelled channel that corresponds to each Xenon L edge. The feature can be fit with a gaussian of equivalent width ~ 70 eV, the exact value depending on the detector.

The overall response can be increased with the area_factor keyword. The default value is 1.0, with the assumption that the geometric area will be included through use of an ancilliary response file (George et al 1992) generated by xpcaarf. Since current versions of that tool, however, contain only geometric response (corrected for pointing direction) and no energy dependent terms, the effective area can be brought in through this parameter. This is a convenience for users run pcarmf outside of pcarsp.

The flag LBL_sigma (which takes values of 0.0 or 1.0) controls which parameterization of Xenon cross sections is used. The default (0.0) uses polynomial approximations to the data of Henke et al 1982 below 10 keV and Veigele 1973 above 10 keV. Setting LBL_sigma=1.0 uses data from Henke et al. 1993 below 30 keV. We find the results quite similar; the availability of updated data from Henke et al. 1993 motivated us to explore the importance of a small discontinuity in the adopted cross sections near 10 keV. *how did the mylar/propane 2% discontinuity at 10 keV get resolved?*

REFERENCES

Dias, T. H. V. T., Santos, F. P., dos Santos, J. M. F., Lopes, J. A. M., Veloso, J. F. C. A., Rachinhas, P. J. B. M., Morgado, R. E., Stauffer, A. D., and Conde, C. A. N. 1996, IEEE Trans. Nucl. Sci, NS-43, 1432.

Dias, T. H. V. T., dos Santos, J. M. F., Rachinhas, P. J. B. M., Santos, F. P., and Conde, C. A. N. 1997, J. Appl. Phys. 82(6), 2742.

Glasser, C. A., Odell, C. E., and Seufert, S. E., 1994, IEEE Trans. Nucl. Sci., NS-41(4), 1343.

oh happily we f-tool.

Fraser, G. W., 1989, "X-ray Detectors in Astronomy", (Cambridge University Press:Cambridge, Great Britain)

George, I. M., Arnaud, K. A., Pence, B., and Ruamsuwan, L. 1992, Legacy, 2, 51. (also http://heasarc.gsfc.nasa.gov/docs/journal/calibration_rqmts2.html)

Giles, A. B. 1995, "PCA Housekeeping - Status, Use, Screen Functions, Recall,Modes, Soc Interface", document PCA-HK-EXP v6.1, also available at http://lheawww.gsfc.nasa.gov/docs/xray/xte/pca/doc2/HKstatus.ps.

Hatsukade, I. and Tsunemi, H. 1991, in "Frontiers of X-ray Astronomy", eds. Y. Tanaka and K. Koyama, proceedings of Yamada Conference XXVIII, p. 387 (ISBN 4-946443-11-8).

Henke, B. L., Lee, P., Tanaka, T. J., Shimabukuro, R. L., and Fujikawa, B. K. 1982, Atomic Data and Nuclear Data Tables, 27, 1.

Henke, B. L., Gullikson, E. M., and Davis, J. C. 1993, Atomic Data and Nuclear Data Tables, 54(2), 181.

Host, S. S., Gotthelf, E. V., Tsunemi, H., and Negoro, H. 1994, PASJ, 46, L151.

Inoue, H., Koyama, K., Matsuoka, M., Ohashi, T., Tanaka, Y., and Tsuenemi, H. 1978, Nucl. Instrum. Meth., A157, 295.

Jahoda, K. and McCammon, D. 1988, Nucl. Instrum. Meth., A272, 800.

Jahoda, K., Swank, J. H., Giles, A. B., Stark, M. J., Strohmayer, T., Zhang, W., and Morgan, E. H. 1996, Proc. SPIE 2808: EUV, X-ray, and Gamma-ray Instrumentation for Astronomy VII, 59.

Jahoda, K., Stark, M. J., Strohmayer, T. E., Zhang, W., Morgan, E. H., and Fox, D. 1998, Nuclear Physics B Proceedings Supplements. Eds. L. Scarsi, H. Bradt, P. Giommi, and F. Fiore, in press.

Rothschild, R., E., Blanco, P. R., Gruber, D. E., Heindl, W. A., MacDonald, D. R., Marsden, D. C., Pelling, M. R., Wayne, L. R., and Hink, P. L. 1998, ApJ, 496, in press.

Rots, A. H. et al, 1998, ApJ, accepted

dos Santos, J. M. F., Bento, A. C. S. S. M., and Conde, C. A. N. 1994, Nucl. Instrum. Meth., A337, 427.

dos Santos, J. M. F., Morgando, R. E., Tavora, L. M. N., and C. A. N. 1994, Nucl. Instrum. Meth., A350, 216.

http://legacy.gsfc.nasa.gov/docs/xte/abc/time_tutorial.html

Tomsick, J. A. and Kaaret, P. 1998, http://lheawww.gsfc.nasa.gov/users/keith/tomsick.ps.

Veigele, W. J., 1973, Atomic Data Tables, 5, 51.

Weaver, K. A., Krolik, J. H., and Pier, E. A. 1998, ApJ, 498, in press (astro-ph/9712035).

Zhang, W. et al 1994, Proc. SPIE 2006: EUV, X-ray, and Gamma-ray Instrumentation for Astronomy IV, 324.

Zhang, W., Jahoda, K., Swank, J. H., Morgan, E. H., and Giles, A. B. 1995, ApJ, 449, 930.

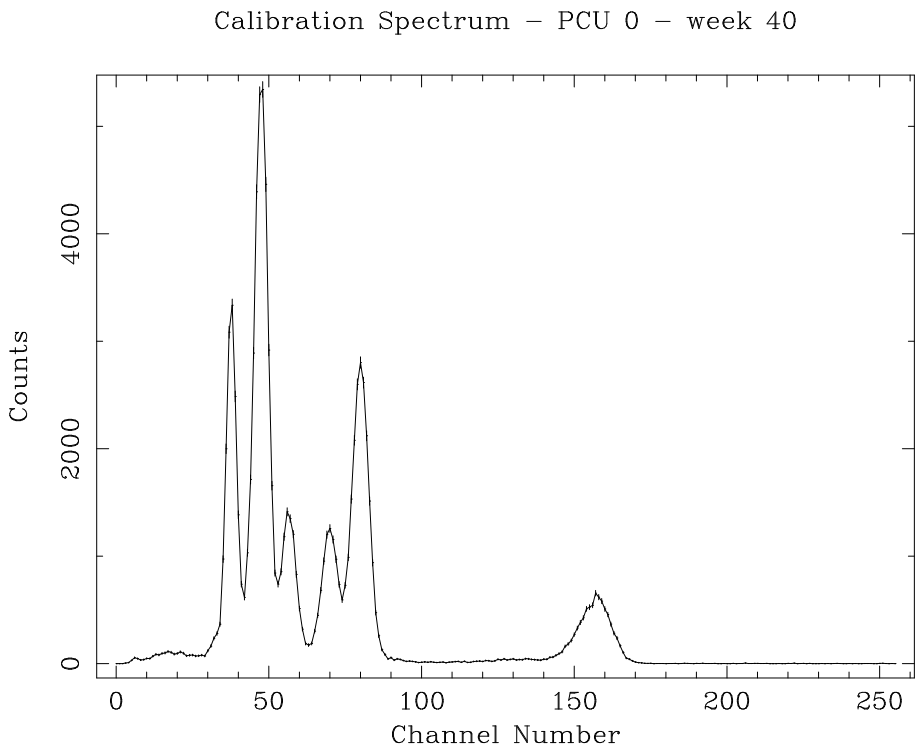

Fig. 1.— Calibration spectrum from PCU 0

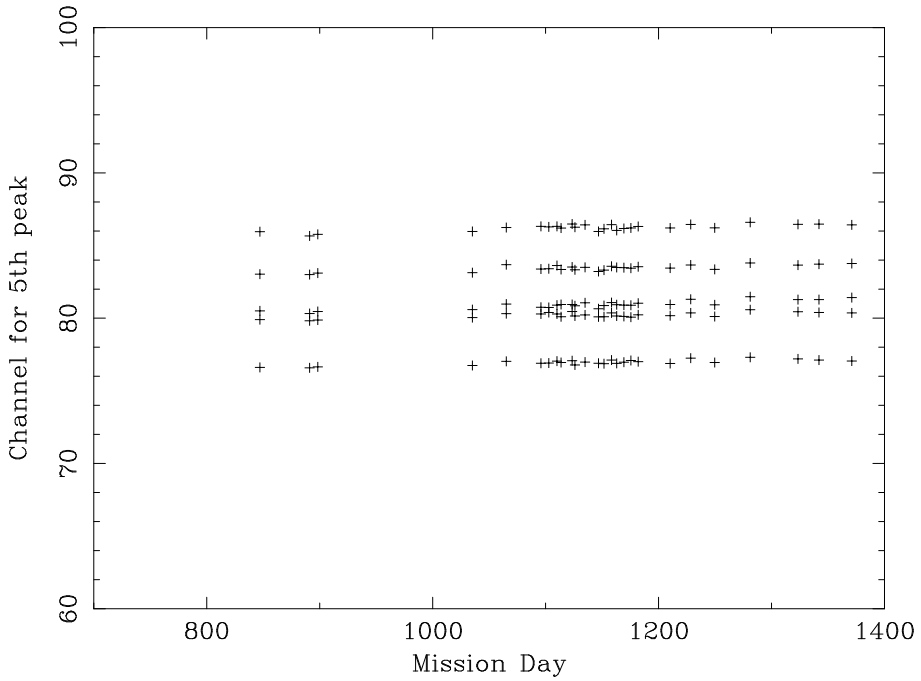

Fig. 2.— Peak channel fit to the 30 keV calibration peak

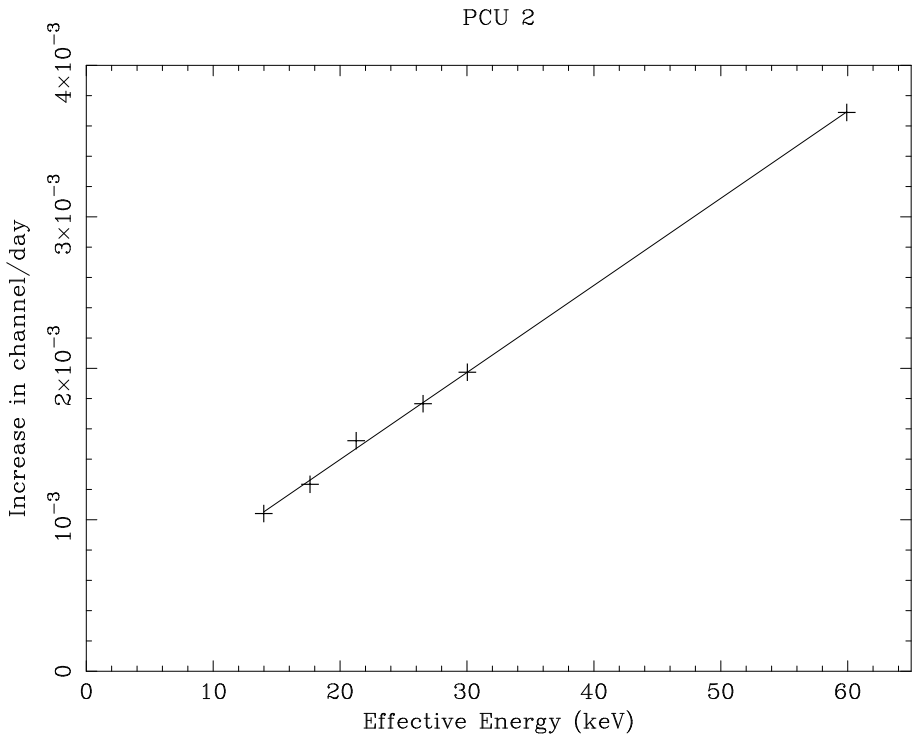

Fig. 3.— Slope of the channel vs time relationships, plotted as a function of effective energy along with a linear fit.

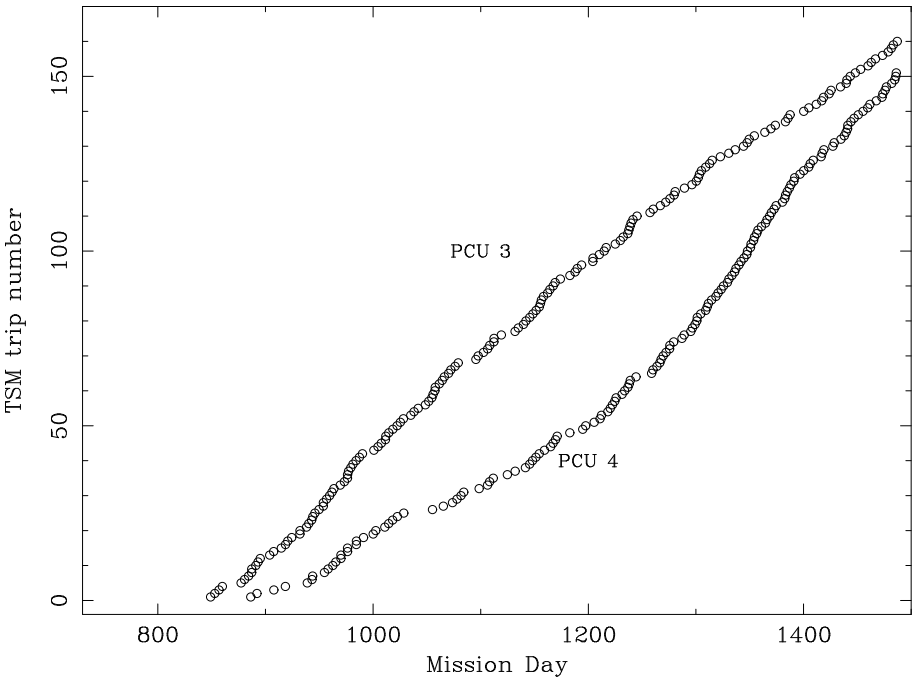

Fig. 4.— Integral trip off distribution for PCU 3 and 4

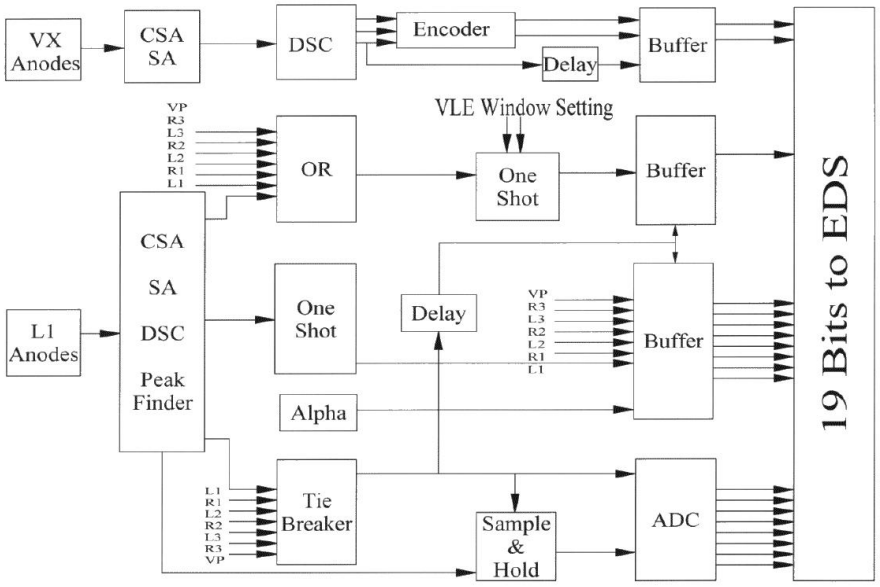

Fig. 5.— Schematic diagram of the PCU timing logic

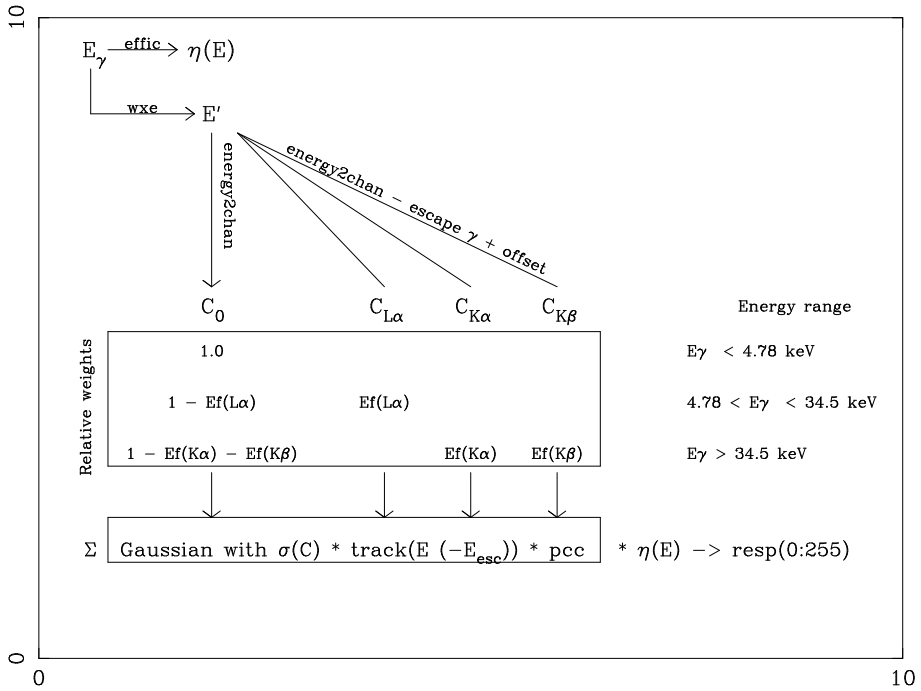

Fig. 6.— Elements of the response matrix

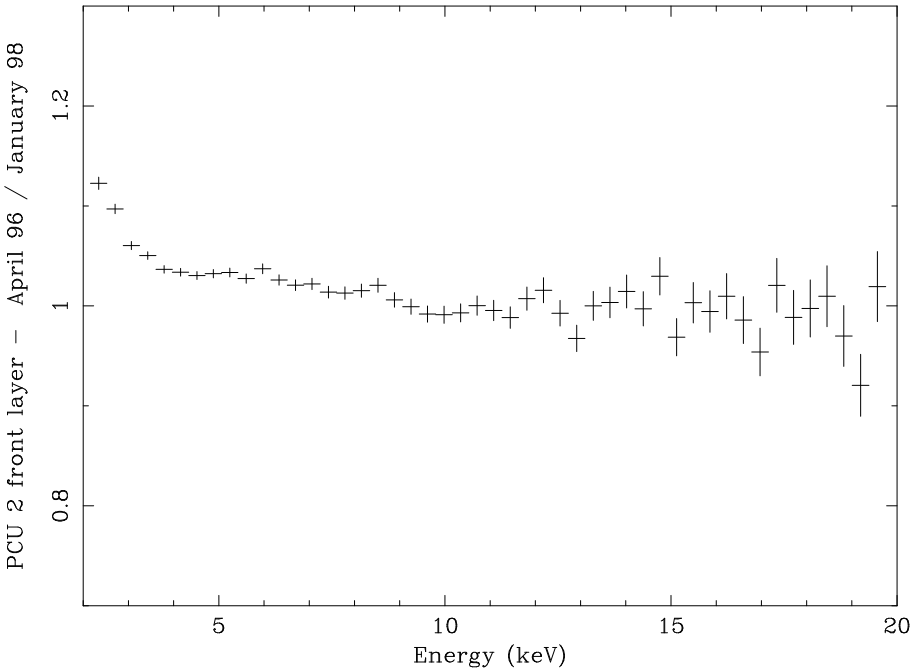

Fig. 7.— Ratio ob counts observed from the Crab Nebula in January 1998 and April 1996. Data shown is from PCU 2, front layer.

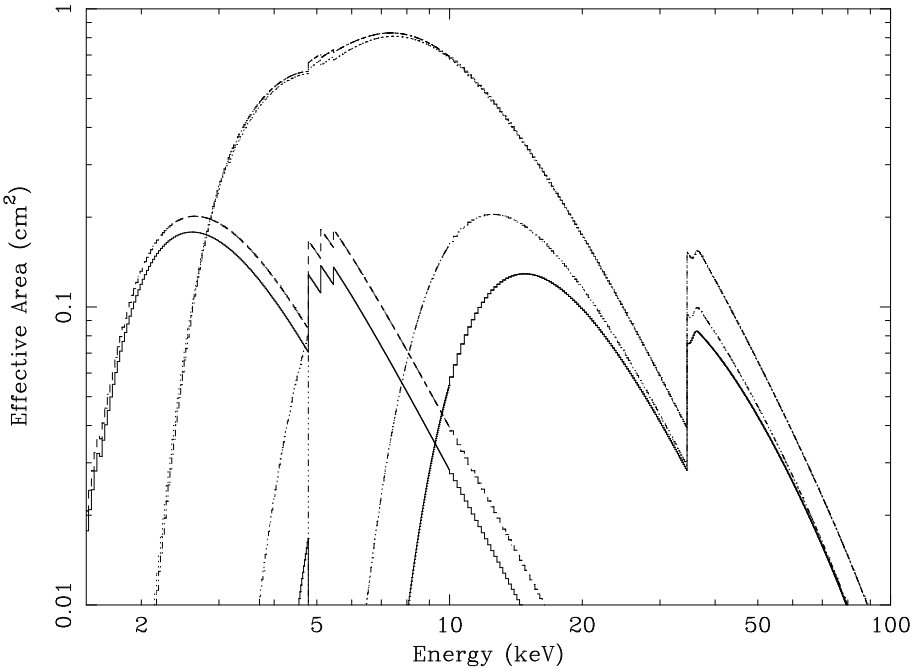

Fig. 8.— Quantum efficiencies for different layers in PCU 0. Shown are the propane and first xenon layer efficiencies for May 1996 and January 1998 along with the xenon efficiencies for the second and third layers in January 1998. Note that between 3 and 10 keV almost all of the efficiency is in the first layer; above 15 keV the inner layers become comparable to the first layer. The jump in the propane layer efficiency at 4.78 keV is due to the presence of xenon in this layer.

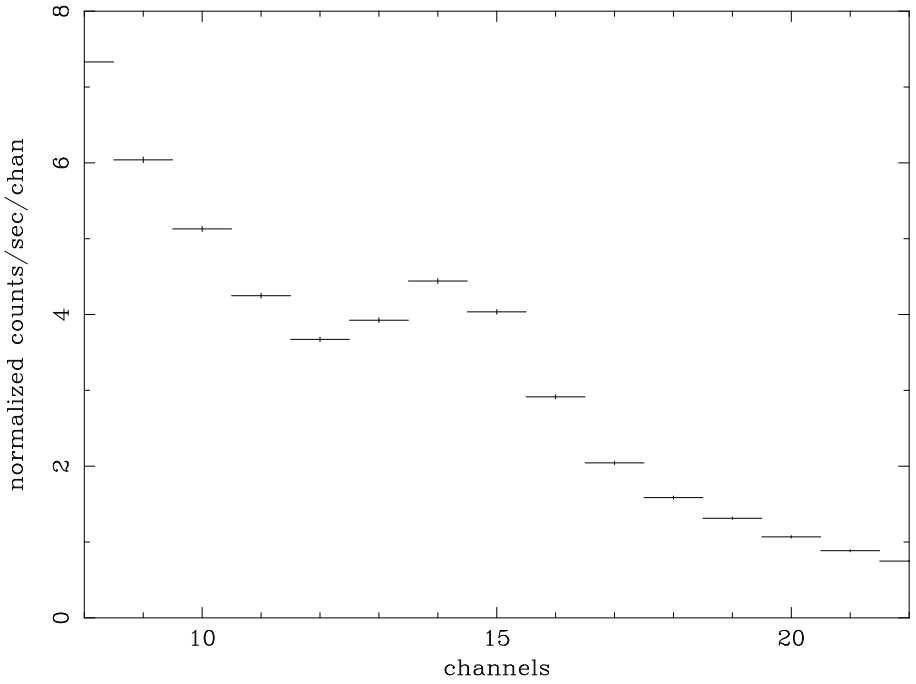

Fig. 9.— Count spectrum from Cas-A, showing the 6.59 keV Iron line

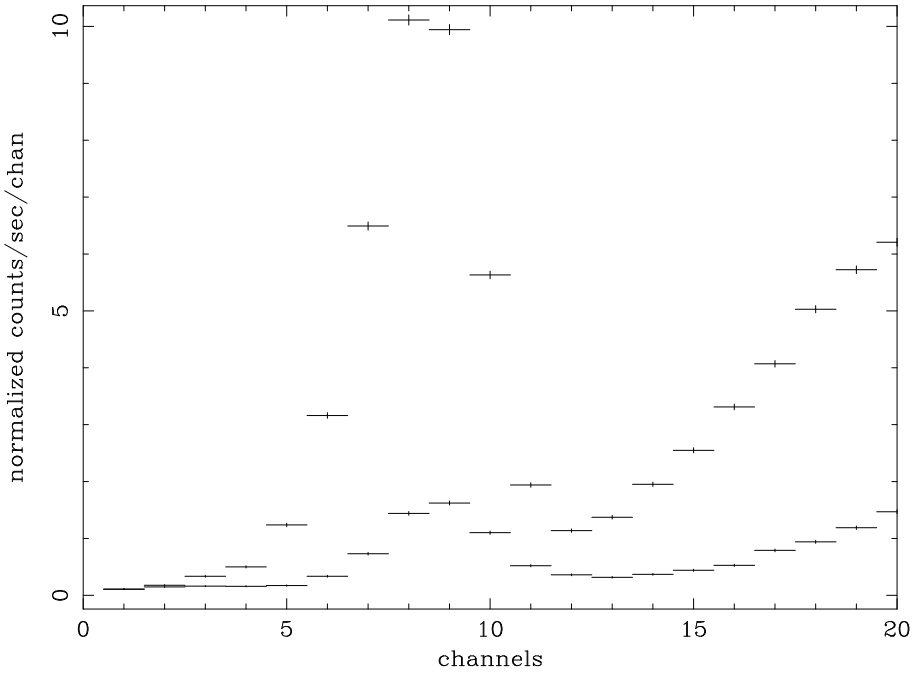

Fig. 10.— Count spectrum from the Crab as observed in the second and third layers; the edge at 4.78 keV shows as peak in channels near 10.

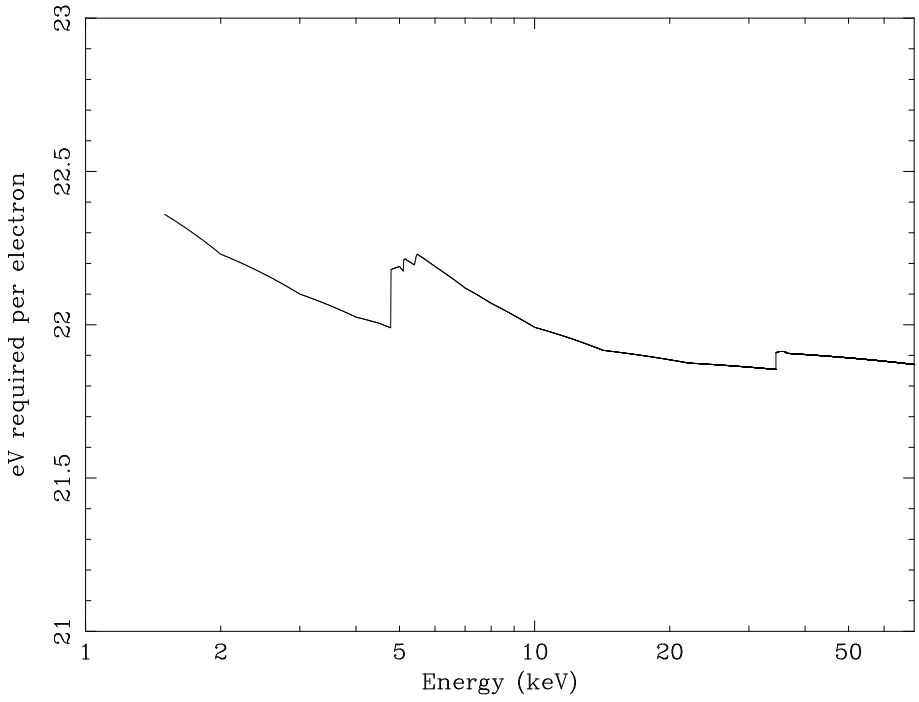

Fig. 11.— The number of eV required to produce one electron as a function of photon energy

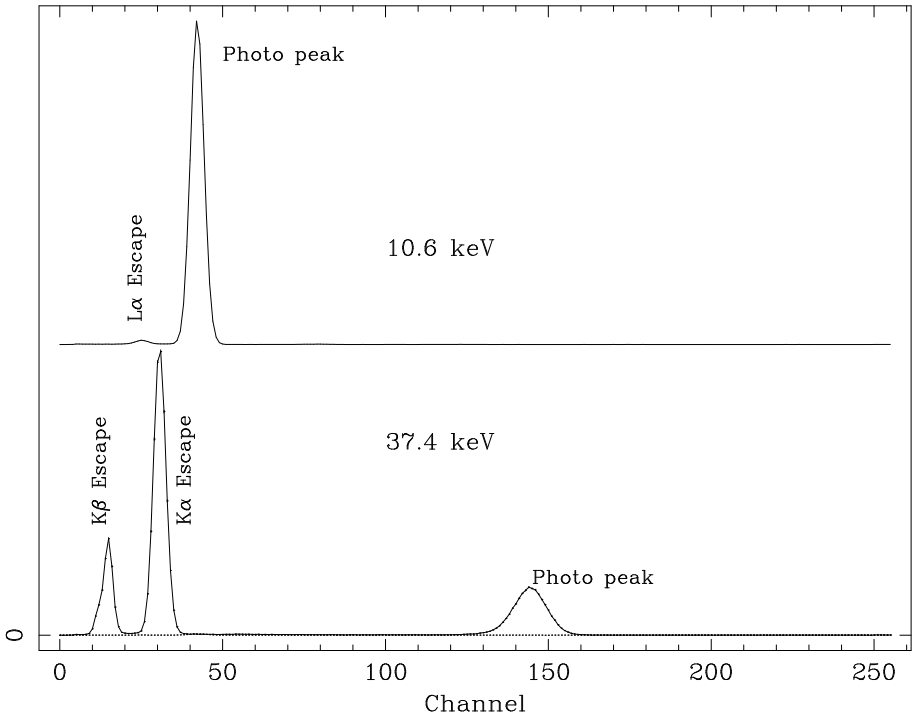

Fig. 12.— Channel spectra from representative ground calibration lines.

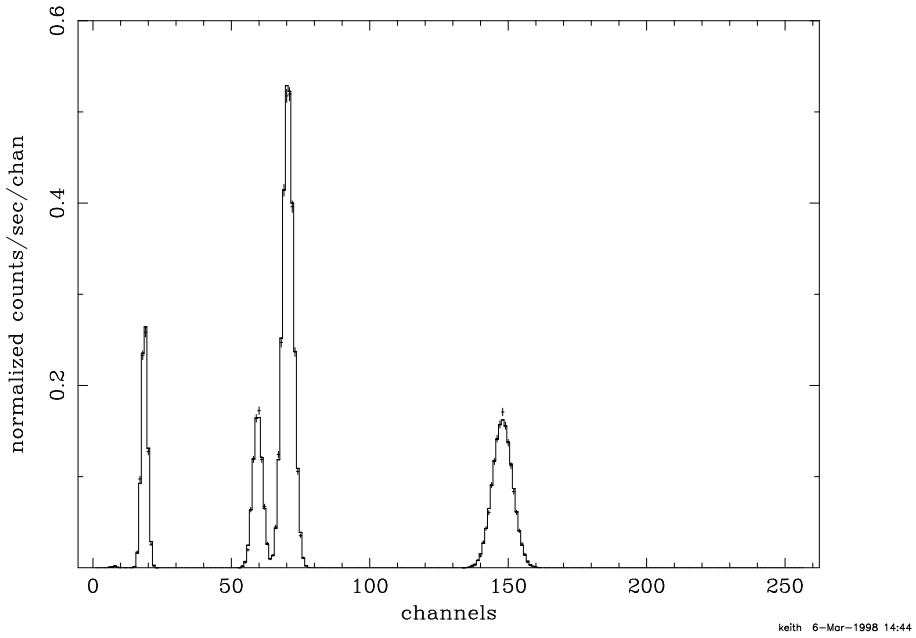

Fig. 13.— Model response to two lines at 6.5 and 55 keV. Channels correspond to epoch 3 high voltage setting.

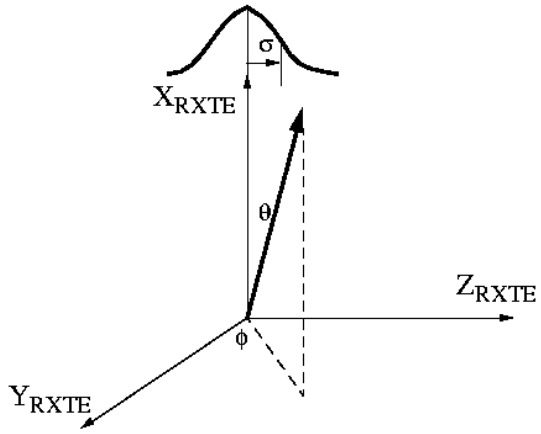

Fig. 14.— Geometry of the the collimator model

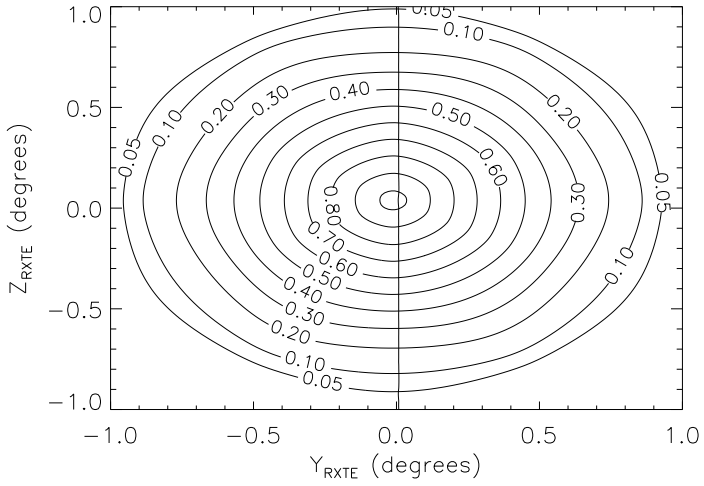

Fig. 15.— Collimator transmission for PCU 0 in spacecraft coordinates

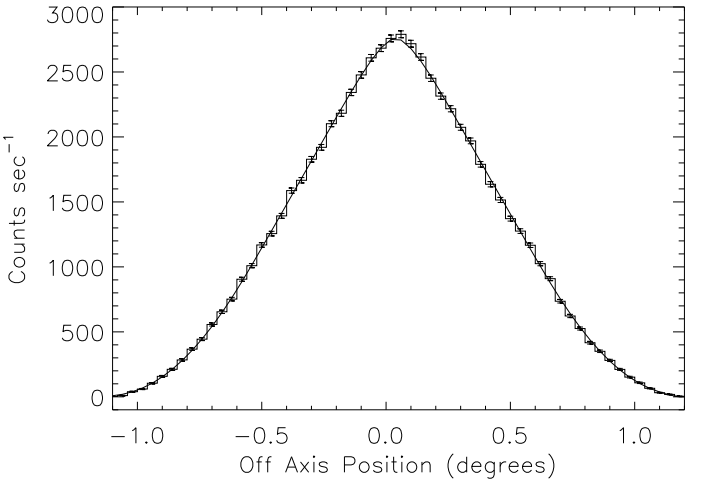

Fig. 16.— Observed counting rate and collimator model for scan over Crab Nebula

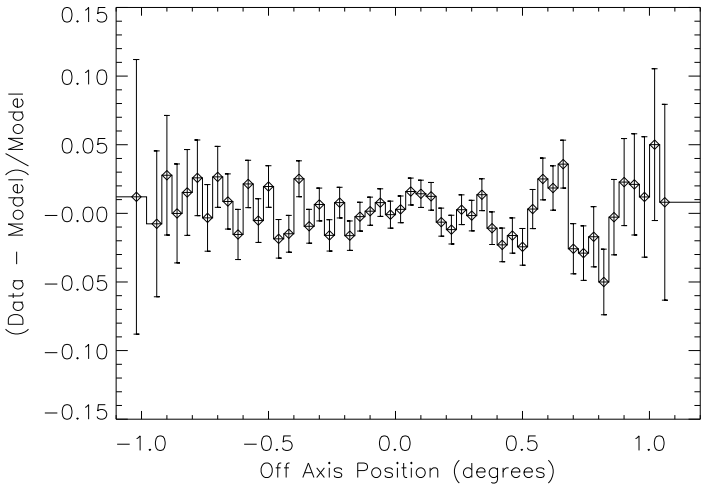

Fig. 17.— Ratio of Counting rate to collimator model for scan over Crab Nebula

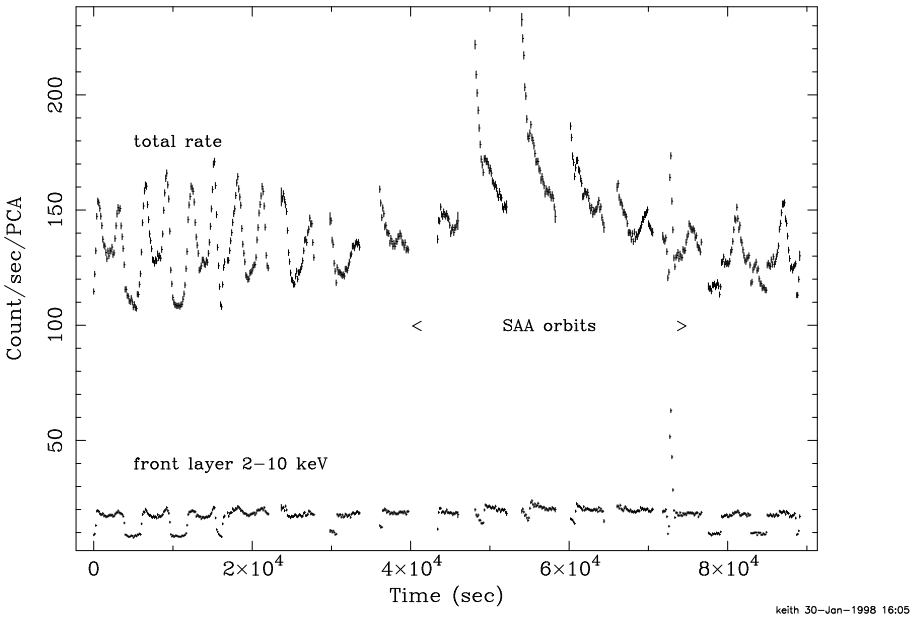

Fig. 18.— Background variation over a day

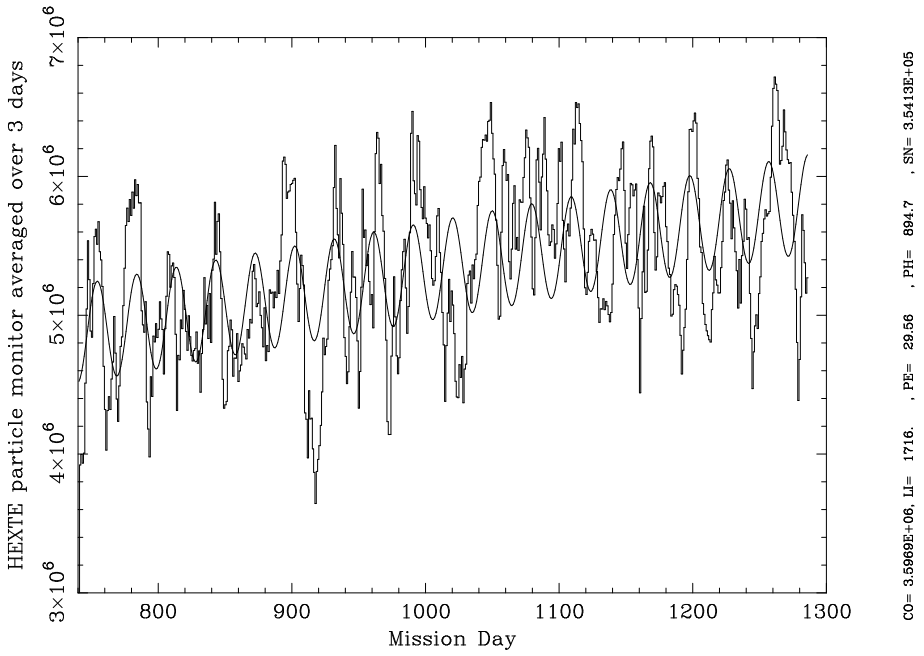

Fig. 19.— HEXTE particle monitor rate vs time. The particle monitor is the only instrument which remains on through the SAA, and provides a monitor of total radiation dose. Trends are discussed in the text.

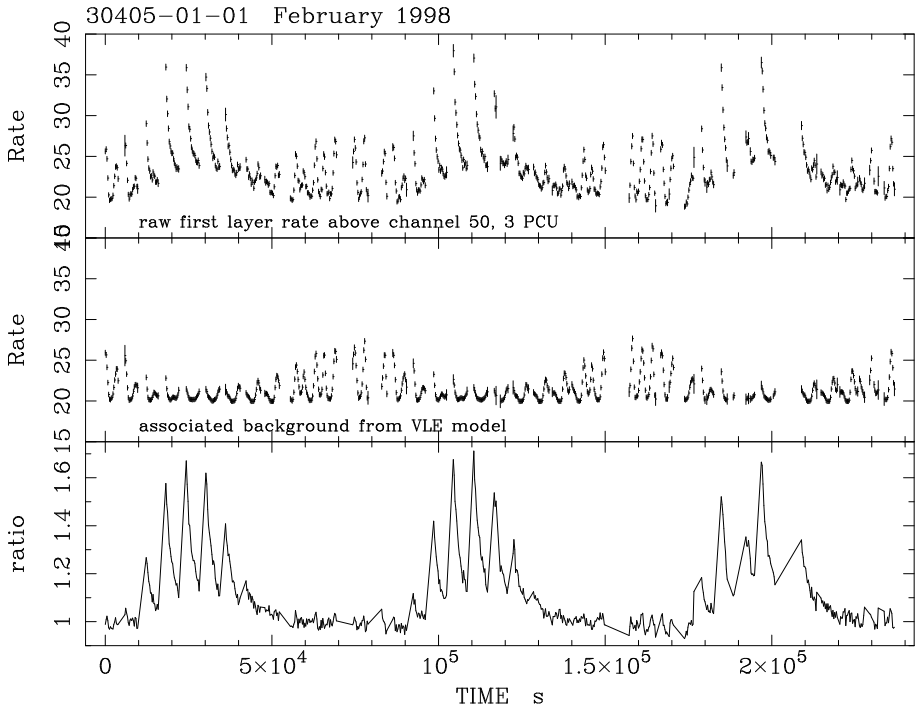

Fig. 20.— Raw observed rate from the first layer of PCU 0, 1, and 2 in channels 51-249 (top panel); VLE background model corresponding to this data (middle panel); and the ratio of data/model (bottom panel). The VLE background model does well at reproducing the large variations in non SAA orbits, but clearly misses an activation component during the SAA orbits.

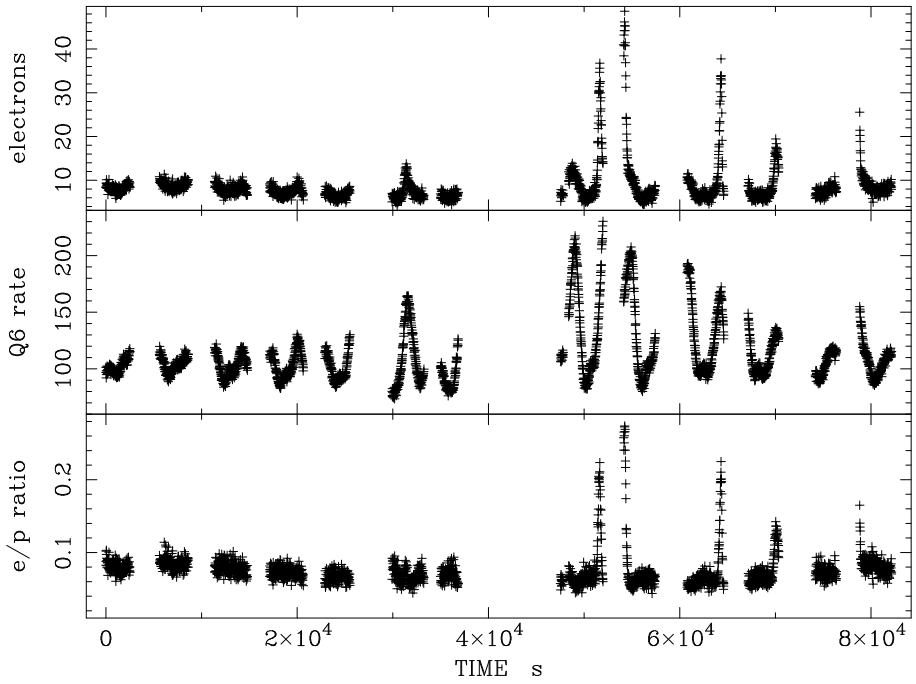

Fig. 21.— Rates proportional to he electron rate, the proton rate, and the ratio of the two.

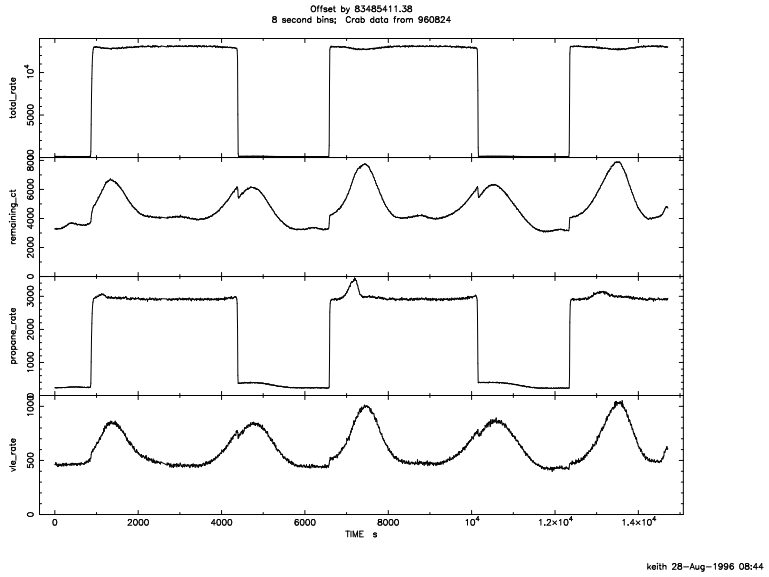

Fig. 22.— Rates from Standard 1 data in 8 second bins. All detector activity passed to EDS is ocunted in one of these rates exactly once.

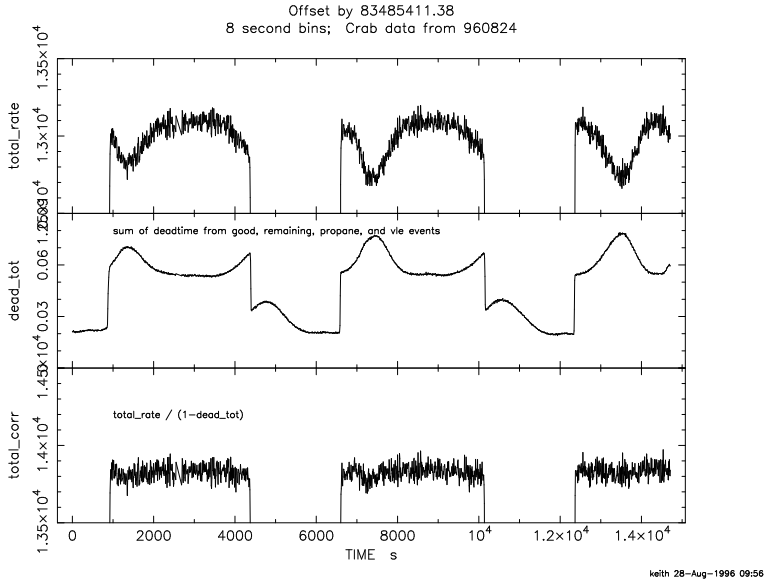

Fig. 23.— Rate, total deadtime, and deadtime corrected rate for Crab, expanded vertical scale.

Table 1. Gain and offset values for the PCA

Date [a]	PCU 0		PCU 1		PCU 2		PCU 3		PCU 4	
	gain	offset	gain	offset	gain	offset	gain	offset	gain	offset
12/30/95:00:00:00	24	1	22	1	29	1	10	0	2	0
01/18/96:18:31:45	0	0	0	0	0	0	0	0	0	0
02/28/96:19:24:40	29	-1	20	-1	27	-1	14	-1	-1	-1
03/25/96:21:02:50	29	-1	20	-1	27	-1	14	-1	33	-1

[a]first data and time for which these settings apply

Table 2. In Flight calibration energies

Energy	Source
13.930	Np - L
17.530	Np - L
21.130	Np - L
26.350	Am^{241}
29.8	blend of Xe escape peak and Xe Kα
59.54	Am^{241}

Table 3. Calibration line channels on Day 0

line	PCU 0	PCU 1	PCU 2	PCU 3	PCU 4
1	37.148	38.805	36.856	40.111	35.648
2	46.735	49.598	48.481	50.229	44.886
3	55.762	58.000	55.431	59.946	53.425
4	68.990	71.538	68.614	73.919	65.993
5	79.010	81.852	78.668	84.682	75.645
6	154.730	160.224	154.020	165.344	147.712

Table 4. Calibration line channel shift per day

line	PCU 0	PCU 1	PCU 2	PCU 3	PCU 4
1	5.985e-4	6.180e-4	1.041e-3	6.509e-4	6.448e-4
2	7.107e-4	8.491e-4	1.234e-3	9.156e-4	7.104e-4
3	8.727e-4	9.607e-4	1.522e-3	1.025e-3	9.120e-4
4	9.934e-4	1.192e-3	1.766e-3	1.297e-3	1.058e-3
5	1.048e-3	1.312e-3	1.974e-3	1.356e-3	1.148e-3
6	1.608e-3	2.532e-3	3.689e-3	2.433e-3	2.277e-3

Table 5. Nominal PCU dimensions

component	Material	Dimension
Thermal shield	polyimide	76μ
Collimator sheet	BeCu	0.0027 inch (?)
Collimator cell		8 inch (height)
Collimator cell		0.125 inch (flat to flat)
Entrance window	Mylar	0.001 inch
Window coating	Aluminum	$700A$ per side
Anti-coincidence	Propane	1.2 cm
		798 torr at $22\deg C$
Separation window	Mylar	0.001 inch
Window coating	Aluminum	$700A$ per side
Main volume	Xenon (90%)/CH_4 (10%)	836 torr at $22\deg C$
layer 1		1.35 cm
layer 2		1.35 cm
layer 3		1.35 cm
Graded shield	Tantalum	0.060 inch (???)
	Tin	0.020 inch (???)

Table 6. PCU alignements

PCU	y(RXTE)	z(RXTE)	Area
0	-0.0000385	0.000629	0.9912
1	0.0001046	0.000529	0.9947
2	-0.0000500	0.000746	1.0000
3	0.0002940	0.001340	0.9410
4	0.0002900	0.001970	0.9277

Table 7. Items is PCA Standard 1 data

Mnemonic	Data Type	Dimension	unit
Time	D		s
XeCntPcu0	1024I	(1024)	count
XeCntPcu1	1024I	(1024)	count
XeCntPcu2	1024I	(1024)	count
XeCntPcu3	1024I	(1024)	count
XeCntPcu4	1024I	(1024)	count
RemainingCnt	1024I	(1024)	count
VpCnt	1024I	(1024)	count
VLECnt	1024I	(1024)	count
CalX1LSpecPcu0	256I	(256)	count
CalX1RSpecPcu0	256I	(256)	count
CalX2LSpecPcu0	256I	(256)	count
CalX2RSpecPcu0	256I	(256)	count
CalX3LSpecPcu0	256I	(256)	count
CalX3RSpecPcu0	256I	(256)	count
CalX1LSpecPcu1	256I	(256)	count
CalX1RSpecPcu1	256I	(256)	count
CalX2LSpecPcu1	256I	(256)	count
CalX2RSpecPcu1	256I	(256)	count
CalX3LSpecPcu1	256I	(256)	count
CalX3RSpecPcu1	256I	(256)	count
CalX1LSpecPcu2	256I	(256)	count
CalX1RSpecPcu2	256I	(256)	count
CalX2LSpecPcu2	256I	(256)	count
CalX2RSpecPcu2	256I	(256)	count
CalX3LSpecPcu2	256I	(256)	count
CalX3RSpecPcu2	256I	(256)	count
CalX1LSpecPcu3	256I	(256)	count
CalX1RSpecPcu3	256I	(256)	count
CalX2LSpecPcu3	256I	(256)	count
CalX2RSpecPcu3	256I	(256)	count
CalX3LSpecPcu3	256I	(256)	count
CalX3RSpecPcu3	256I	(256)	count
CalX1LSpecPcu4	256I	(256)	count
CalX1RSpecPcu4	256I	(256)	count
CalX2LSpecPcu4	256I	(256)	count

Table 7—Continued

Mnemonic	Data Type	Dimension	unit
CalX2RSpecPcu4	256I	(256)	count
CalX3LSpecPcu4	256I	(256)	count
CalX3RSpecPcu4	256I	(256)	count
Spillage	B		Count
ModeSpecific	B		Count

Table 8. Items is PCA Standard 2 data

Mnemonic	Index	Dimension	unit
Time	D		s
X1LSpecPcu0	(0:128)	(129)	count
X1RSpecPcu0	(0:128)	(129)	count
X2LSpecPcu0	(0:128)	(129)	count
X2RSpecPcu0	(0:128)	(129)	count
X3LSpecPcu0	(0:128)	(129)	count
X3RSpecPcu0	(0:128)	(129)	count
VpSpecPcu0	(0:32)	(33)	count
VLECntPcu0	1		count
VpX1LCntPcu0	2		count
VpX1RCntPcu0	3		count
VxX1LCntPcu0	4		count
VxX1RCntPcu0	5		count
VxX2LCntPcu0	6		count
VxX2RCntPcu0	7		count
VxX3LCntPcu0	8		count
VxX3RCntPcu0	9		count
X1LX1RCntPcu0	10		count
X2LX2RCntPcu0	11		count
X3LX3RCntPcu0	12		count
Q3VxVpXeCntPcu0	13		count
Q4VxVpXeCntPcu0	14		count
Q5VxVpXeCntPcu0	15		count
Q6VxVpXeCntPcu0	16		count
Q7VxVpXeCntPcu0	17		count
Q8VxVpXeCntPcu0	18		count
CALCntPcu0	19		count
VxLCntPcu0	20		count
VxHCntPcu0	21		count
VxLVxHCntPcu0	22		count
VpXe23CntPcu0	23		count
X1LX2LCntPcu0	24		count
X1RX2RCntPcu0	25		count
X2LX3LCntPcu0	26		count
X2RX3RCntPcu0	27		count
VxpXOR2XeCntPcu0	28		count

Table 8—Continued

Mnemonic	Index	Dimension	unit
ZeroCntPcu0	29		count
Spillage			Count
ModeSpecific			Count

Table 9. Default parameters for PCARMF v3.0

Mnemonic	query	Value
outfile	q	rossi.rmf
pcuid	q	0-4
lld_code	q	63[a]
e2c_model	h	3
e2cfile	h	CALDB
nofits	h	0[b]
scale_hack	h	0
scale_file	h	none
chatter	h	10
date	q	960503
clobber	h	yes
xe_gm_cm2_l1_p0	h	0.00790
xe_gm_cm2_l2_p0	h	0.0064
xe_gm_cm2_l3_p0	h	0.0064
xe_gm_cm2_pr0	h	1.6e-04
xe_gm_cm2_l1_p1	h	0.00790
xe_gm_cm2_l2_p1	h	0.0064
xe_gm_cm2_l3_p1	h	0.0064
xe_gm_cm2_pr1	h	1.7e-04
xe_gm_cm2_l1_p2	h	0.00790
xe_gm_cm2_l2_p2	h	0.00640
xe_gm_cm2_l3_p2	h	0.00640
xe_gm_cm2_pr2	h	1.5e-04
xe_gm_cm2_l1_p3	h	0.00790
xe_gm_cm2_l2_p3	h	0.0064
xe_gm_cm2_l3_p3	h	0.0064
xe_gm_cm2_pr3	h	1.8e-04
xe_gm_cm2_l1_p4	h	0.00810
xe_gm_cm2_l2_p4	h	0.0066
xe_gm_cm2_l3_p4	h	0.0066
xe_gm_cm2_pr4	h	1.7e-04
xe_kedge_veto	h	0.81
pr_gmcm2	h	0.00261
my_gmcm2_p0	h	0.00708
my_gmcm2_p1	h	0.00708
my_gmcm2_p2	h	0.00648

Table 9—Continued

Mnemonic	query	Value
my_gmcm2_p3	h	0.00648
my_gmcm2_p4	h	0.00708
al_gmcm2	h	7.6e-5
xeKedge	h	34.561
xeL3edge	h	4.782
xeL2edge	h	5.104
xeL1edge	h	5.453
EscFracKb	h	0.155
EscFracKa	h	0.545
EscFracL1	h	0.010
EscFracL2	h	0.000
EscFracL3	h	0.000
EscFracLt	h	0.009
EscEnerKa	h	29.70
EscEnerKb	h	33.62
EscEnerLa	h	4.110
DeltaE_L3	h	0.085
DeltaE_L2	h	0.032
DeltaE_L1	h	0.012
DeltaE_K	h	0.180
delta_el_L	h	3.9
delta_el_Ka	h	-2.26
delta_el_Kb	h	3.84
LBL_sigma	h	0.00
area_factor	h	1.0
epoint	h	16.0
track_coeff	h	0.015
resolution_factor	h	0.80
pcc_coeff	h	0.001
gain_stretch	h	1.000
date0_0	h	960416
date0_1	h	960416
date0_2	h	960416
date0_3	h	960416
date0_4	h	960416
gain_shift_offset0	h	3.755e-04

Table 9—Continued

Mnemonic	query	Value
gain_shift_slope0	h	2.113e-05
gain_shift_offset1	h	9.158e-05
gain_shift_slope1	h	4.082e-05
gain_shift_offset2	h	2.487e-04
gain_shift_slope2	h	5.745e-05
gain_shift_offset3	h	2.269e-04
gain_shift_slope3	h	3.729e-05
gain_shift_offset4	h	1.107e-04
gain_shift_slope4	h	3.593e-05
xe_pr_daily_change0	h	9.35e-08
xe_pr_daily_change1	h	4.67e-08
xe_pr_daily_change2	h	1.09e-07
xe_pr_daily_change3	h	1.56e-08
xe_pr_daily_change4	h	4.67e-08
resp1_0	h	0.0
resp2_0	h	0.0
resp1_1	h	0.0
resp2_1	h	0.0
resp1_2	h	0.0
resp2_2	h	0.0
resp1_3	h	0.0
resp2_3	h	0.0
resp1_4	h	0.0
resp2_4	h	0.0

[a]1=L1, 2=R1, 3=LR1, 12=LR2, 48=LR3, 63=Xenon total, 64=Propane

[b]see text for specific format rules